Transcriptomic response of citrus psyllid salivary glands to the infection of citrus Huanglongbing pathogen

San-Tao Zhao[1,2,3] (ID), Xiao-Tong Ran[1,3], Yu-Yang Huang[1,2], Wen Sang[1,2], Bugenimana Eric Derrick[4] and Bao-Li Qiu[1,2,3] (ID)

[1]Engineering Research Centre of Biological Control, Ministry of Education, South China Agricultural University, Guangzhou 510642, China; [2]Guangdong Laboratory for Lingnan Modern Agriculture, Guangzhou 510642, China; [3]Engineering Research Center of Biotechnology for Active Substances, Ministry of Education, Chongqing Normal University, Chongqing 401331, China and [4]College of Agriculture and Animal Husbandry, University of Rwanda, Kigali 999051, Rwanda

Abstract

The Asian citrus psyllid, *Diaphorina citri* Kuwayama (Hemiptera: Psyllidae), is the key vector insect transmitting the *Candidatus* Liberibacter asiaticus (*C*Las) bacterium that causes the devastating citrus greening disease (Huanglongbing, HLB) worldwide. The *D. citri* salivary glands (SG) exhibit an important barrier against the transmission of HLB pathogen. However, knowledge on the molecular mechanism of SG defence against *C*Las infection is still limited. In the present study, we compared the SG transcriptomic response of *C*Las-free and *C*Las-infected *D. citri* using an illumine paired-end RNA sequencing. In total of 861 differentially expressed genes (DEGs) in the SG upon *C*Las infection, including 202 upregulated DEGs and 659 downregulated DEGs were identified. Functional annotation analysis showed that most of the DEGs were associated with cellular processes, metabolic processes, and the immune response. Gene ontology and Kyoto Encyclopaedia of Genes and Genomes enrichment analyses revealed that these DEGs were enriched in pathways involving carbohydrate metabolism, amino acid metabolism, the immune system, the digestive system, the lysosome, and endocytosis. A total of 16 DEGs were randomly selected to further validate the accuracy of RNA-Seq dataset by reverse-transcription quantitative polymerase chain reaction. This study provides substantial transcriptomic information regarding the SG of *D. citri* in response to *C*Las infection, which may shed light on the molecular interaction between *D. citri* and *C*Las, and provides new ideas for the prevention and control of citrus psyllid.

Introduction

The citrus greening disease, also known as Huanglongbing (HLB), caused by the phloem-limited, Gram-negative causative bacterium 'Candidatus Liberibacter asiaticus' (CLas), is the most destructive disease of citrus plants worldwide (Hall *et al.*, 2013). It causes tremendous economic losses each year in most citrus-growing regions by reducing fruit yield and quality, promoting tree decline, and eventually results in plant death (Slisz *et al.*, 2012; Munir *et al.*, 2018). Thus HLB has become the most serious threat to the citrus industry for decades worldwide, and the CLas bacterium is currently unculturable, there are no effective prevention and control methods once established (da Graca *et al.*, 2016).

The Asian citrus psyllid (ACP), *Diaphorina citri* Kuwayama, a phloem-sucking pest of citrus, is considered as the major transmitting vector of CLas bacterium, the causal agent of HLB (George *et al.*, 2018). The psyllid transmits HLB pathogen in a persistent propagative manner, and both nymphs and adults can transmit CLas once they acquired CLas at their nymphal stages (Canale *et al.*, 2017; Andrade *et al.*, 2020). The effective control of ACP is recognised as a key measure to prevent HLB spreading, and it is crucial to investigate novel targets and develop new strategies for ACP management (Vanaclocha *et al.*, 2019).

Like other phloem-sucking insects, *D. citri* feed on the phloem sap of citrus plants; both nymphs and adults puncture the epidermis using a specialised piercing-sucking style, and continuously secrete saliva into plant tissues before ingesting juice from the phloem (George *et al.*, 2017). Saliva is primarily derived from salivary glands (SG) and contains a variety of bioactive components with function in food ingestion, digestion, lubrication, tissue penetration, detoxification, and suppressing host plant defences (Perilla-Henao and Casteel, 2016; Aljbory and Chen, 2018). SG, secreting gelling and watery saliva, act as reservoirs and facilitate the transmission of plant pathogens by inoculating saliva into healthy plants via stylet during insect feeding. Many genes and proteins in the SG are associated with the essential biological processes of insect host that facilitate feeding behaviour or repress host immune responses.

Several SG-secreted proteins acting as effector proteins have been reported, such as MED, SP75, Bt56, and vitellogenin (Yang *et al.*, 2017; Matsumoto and Hattori, 2018; Xu *et al.*, 2019; Ji *et al.*, 2021). Additionally, in several vector-borne hemipterans, like *Acyrthosiphon pisum* Harris, *Bemisia tabaci* Gennadius, *Nilaparvata lugens* Stal, and *D. citri* (Carolan *et al.*, 2011; Su *et al.*, 2012; Ji *et al.*, 2013; Yu and Killiny, 2018), SG, and secreted saliva play critical roles mediating interactions among insects, insect-borne pathogens, and their host plants (Perilla-Henao and Casteel, 2016; van Bell and Will, 2016).

The transmission of HLB pathogen by *D. citri* is associated with the properties of SG during insect feeding. Both *D. citri* nymphs and adults can transmit *C*Las by acquiring the pathogen, and the *C*Las-infected psyllids have the ability to transmit HLB pathogen throughout their lives. *C*Las is transmitted by *D. citri* more efficiently when it is acquired by nymphs rather than adults (Mann *et al.*, 2018). Prior studies have reveal that the newly produced pathogen can be detected in various internal organs of *C*Las-infected *D. citri*, including the alimentary canal, haemolymph, filter chamber, midgut, SG, Malpighian tubules, testis, ovaries, muscle, and fat tissues (Ammar *et al.*, 2011*a*; Coletta *et al.*, 2014). Among these tissues, the proportion of infected SG was significantly lower than that of other tissues in the insect body, suggesting that the SG may serve as an important barrier to *C*Las transmission in the psyllid vector (Ammar *et al.*, 2011*b*). After the acquisition, *C*Las is initially reproduced in the alimentary canal, and subsequently migrates from midgut to haemolymph and other tissues (Chen *et al.*, 2022). It eventually moves into SG to proliferate, from where newly produced pathogens will be injected into healthy plant tissues along with saliva when sucking juice from the phloem (Hall *et al.*, 2013; Wu *et al.*, 2016). In this process, the SG may act as the last, and most important, barrier that the pathogen must breach before entry into new plants, suggesting that the SG could play an important role in the transmission of HLB pathogen.

In the last decade, high-throughput RNA-Seq technology has been widely employed to elucidate the molecular mechanisms of insect–pathogen interactions, especially in the research of host cell responses to exogenous pathogenic infection. By comparative transcriptomic analysis, Kaur *et al.* identified a large number of differentially expressed genes (DEGs) associated with metabolic pathways, signal transduction, transport and catabolism, receptors, glucose transporters, α-glucosidases and the uric acid pathway between *B. tabaci* fed on Tomato chlorosis virus (ToCV) infected and uninfected tomato plants (Kaur *et al.*, 2017). By RNA-Seq analysis, Kruse *et al.* investigated the interactions between *C*Las and the ACP gut, and *C*Las exposure resulted in changes in pathways involving the tricarboxylic acid (TCA) cycle, iron metabolism, insecticide resistance, and the insect immune system (Kruse *et al.*, 2017). Yu *et al.* also performed a comparative transcriptome-wide analysis of *D. citri* midgut upon *C*Las infection, and a total of 778 DEGs involved in ubiquitination, the immune response, the ribosome, endocytosis, the cytoskeleton, and insecticide resistance were identified (Yu *et al.*, 2020).

Additionally, the functions and potential roles of the SG in transmission of plant pathogens have been studied in several other hemipteran insects by RNA-Seq and transcriptomic analysis, such as *A. pisum* (Carolan *et al.*, 2011), *B. tabaci* (Su *et al.*, 2012), *Sitobion avenae*, *Empoasca fabae* Harris and *N. lugens* (DeLay *et al.*, 2012; Zhang *et al.*, 2017; Rao *et al.*, 2019). For ACP insect, SG play an important role in HLB pathogen colonisation and transmission. Although a lot of differential genes and proteins in *D. citri* saliva and SG have been identified (Yu and Killiny, 2018; Liu *et al.*, 2021), the functions and properties of these differentially expressed SG components in *C*Las-free and *C*Las-infected psyllid are still limited. The mechanism underlying *C*Las infection in the SG of *D. citri* remains to be addressed.

In the current study, a comparative transcriptomic analysis was performed between the SG in *C*Las-infected and uninfected ACP using an Illumina RNA-Seq technology. An abundance of DEGs in the SG of *D. citri* were identified, revealing their potential roles in response to *C*Las invasion. This study provides valuable transcriptomic data for further studies of functional genes in SG, which will contribute to our understanding of the molecular mechanisms between *C*Las and *D. citri*.

Materials and methods

Citrus psyllid culture

The colony of ACP used in this study was originally collected from a field population on the orange jessamine *Murraya exotica* L. Mant at the Engineering Research Center of Ministry of Education, South China Agricultural University, Guangzhou, China, in September 2020. A subcolony of ACP was reared in mesh cages (60 cm × 60 cm × 90 cm) with environmental conditions of 26 ± 1°C, 65 ± 5% relative humidity, and a 14:10 (light: dark) photoperiod. Healthy *D. citri* adults were inoculated onto *C*Las-infected *Citrus reticulata* Blanco cv. Shatangju and maintained under the same rearing conditions, and they were infected with HLB pathogen by sucking juice from the phloem during feeding.

To calculate the infection rate of *C*Las in ACP population, genomic DNA from the head of individual ACP was extracted using a TIANamp Micro DNA Kit (TIANGEN Biotech, Beijing, China), and a 16S ribosomal DNA fragment of *C*Las was amplified by using specific primer set OI1/OI2c (Shokrollah *et al.*, 2010). Afterwards, agarose gel electrophoresis was conducted to determine the *C*Las infection rate. When the proportion of *C*Las-infected psyllid reached ≥80%, the infected ACPs were collected for tissue dissection.

Tissue collection and total RNA extraction

For SG collection, the uninfected and *C*Las-infected ACP adults (male/female = 1:1) were anaesthetised on ice, and their SG were dissected in ice-cold sterile 1× phosphate-buffered saline (PBS) solution under a stereomicroscope (ZEISS, Germany). After the dissection, SG tissues were washed with precooled diethypyrocarbonate (DEPC) treated water to remove other remaining tissues, then immediately transferred into RNA*later*® stabilisation solution (Invitrogen, USA) and frozen at −80°C. For transcriptome sequencing, each sample consisted of approximately 1000 pairs of SG, and three biological replicates of the *C*Las-infected and uninfected ACP subcolonies were processed. The total RNA of citrus psyllid SG was extracted using a miRNeasy® Micro Kit (QIAGEN, Germany) based on the manufacturer's directions. RNA concentration and purity were analysed using a NanoPhotometer Spectrophotometer (Nanodrop Technologies, USA). The integrity of total RNA was detected by RNase-free agarose gel electrophoresis, and assessed on an Agilent 2100 Bioanalyzer system (Agilent Technologies, Palo Alto, CA, USA). The flowchart of transcriptome experiments used in this study is shown in fig. 1.
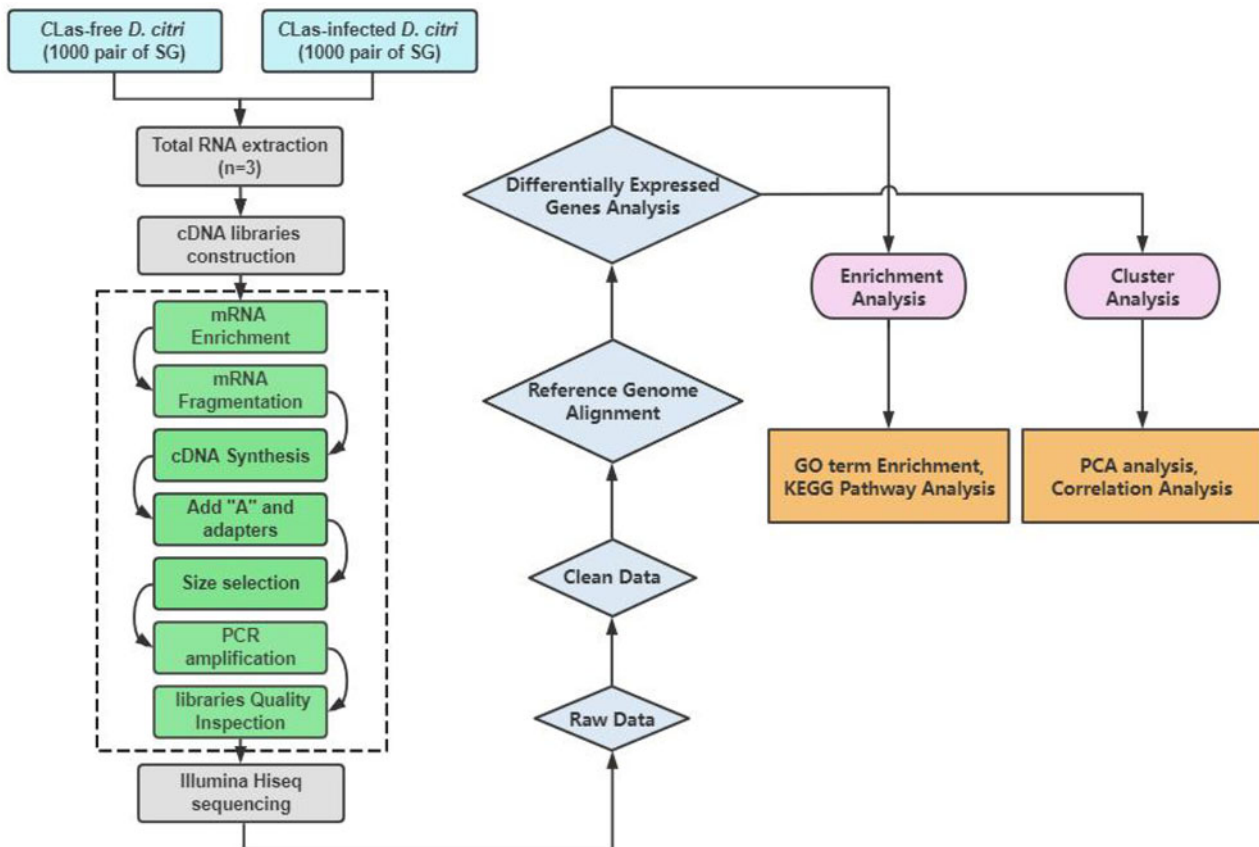
Figure 1. Flowchart illustrating the procedure used in the current study.

cDNA library construction and Illumina sequencing

After quality inspection, the mRNA of citrus psyllid SG was separated from total RNA with oligo (dT) beads (Epicentre, Madison, WI, USA), and the enriched mRNA was then fragmented into approximately 200–700 nt RNA short fragments by using RNA Fragmentation Reagents (Invitrogen, USA). The cDNA was synthesised using the NEBNext® Ultra™ II RNA Library Prep Kit for Illumina® (New England Biolabs, Ipswich, MA, USA) following the instruction manual. The bead-purified double-stranded cDNA fragments were subjected to end repair, 'A' base added, and then ligated into Illumina sequencing adapters. The ligation reaction was purified with the AMPure XP Beads (Beckman Coulter, Brea, CA, USA), and subsequently was size-selected by agarose gel electrophoresis and polymerase chain reaction (PCR) amplification. The quality of library was monitored on the Agilent 2100 Bioanalyzer system, and the concentration was assessed by Qubit® 2.0 Fluorometer (Invitrogen, USA). After the index cluster generation, the resulting cDNA libraries were then deep-sequenced using an Illumina Hiseq™ 4000 platform, and 2×150 bp paired-end reads were generated.

Data filtering and read mapping

The raw reads of FASTQ format were produced from the sequencing data using CASAVA software. Raw sequencing reads were monitored for quality using fastp software (v0.18.0), and Q20, Q30, fuzzy base ratio, error rate, and the GC content of raw data were calculated simultaneously. The clean reads were obtained by removing reads containing adapters, poly A/T tail, reads containing more than

10% of unknown nucleotides (poly-N), and low-quality reads containing more than 50% of low-quality bases (Q-value ≤20). To build the index of the reference genome, the paired-end clean reads were mapped to the *D. citri* reference genome (Genome assembly version 1.1, NCBI RefSeq sequence: GCF_000475195.1) using HISAT2 (v2.2.4) with '-rna-strandness RF' and other parameters set as default. The mapped reads were then assembled by using StringTie (v1.3.1) in a reference-based approach.

Relationship analysis of SG transcriptome samples

To evaluate the reliability and operational stability of the SG transcriptome samples from *C*Las-free and *C*Las-infected ACP, correlation analysis was conducted by R Correlation. The Pearson's correlation coefficient R^2 between two SG transcriptomes was calculated based on fragments per kilo bases per million (FPKM) values. The closer R^2 gets to 1, the better the repeatability between two parallel experiments. Furthermore, a principal component analysis (PCA) from the SG transcriptomes was performed with R package gmodels according to the gene expression of correlated variables. Samples from different effective treatments tend to exhibit separate aggregated distributions, and the more similar of the sample compositions in each treatment, the closer the distance reflected in the PCA diagram.

Identification of DEGs

For each transcription region, a FPKM value was calculated to estimate its expression abundance and variations by RSEM.

DESeq2 R software (v1.16.1) was used to perform differential expression analysis between *C*Las-free and *C*Las-infected subcolonies. The transcripts with the parameter of a false-discovery rate (FDR)-adjusted *P*-value <0.05 and an absolute value log 2(fold-change) of 0 were defined as the threshold for significantly differential expressed.

Gene ontology (GO) and Kyoto Encyclopaedia of Genes and Genomes (KEGG) enrichment analysis of DEGs

GO functional annotation of DEGs between the SG of *C*Las-infected and uninfected ACP was conducted by the topGO package. All DEGs were mapped to GO terms in the GO database, and GO terms with a FDR-corrected *P*-value <0.05 were defined as significantly enriched. KEGG pathway enrichment analysis for DEGs was implemented by using the clusterProfiler R package, and a corrected *P*-value of 0.05 was set as the threshold for significantly enriched pathways in DEGs.

Reverse-transcription quantitative PCR (RT-qPCR) analysis of DEGs

The transcript abundance of 16 selective DEGs was analysed by RT-qPCR. Primer-BLAST program was used to design specific RT-qPCR primers, and all of the primers used are listed in Supplementary table S1. The first strand cDNA was synthesised with approximately 1 µg total RNA of each sample by using the PrimerScript™ RT reagnet Kit with gDNA Eraser (Perfect Real Time) (Takara, Dalian, China). RT-qPCR reactions were carried out using TB Green® Premix Ex Taq™ II (Tli RNaseH Plus) (Takara, Dalian, China), and the reaction mixture contained 5 µl of Premix Ex TaqII (2×), 0.5 µl of forward primer (10 µM), 0.5 µl of reverse primer (10 µM), 1 µl of cDNA template, and 3 µl of double-distilled water (ddH$_2$O) in a final reaction volume of 10 µl. qPCR was performed with the CFX96 Real-Time PCR Detection System (Bio-Rad, USA), and the standard thermal cycle parameters were as follows: 95°C for 2 min; 40 cycles of 95°C for 15 s, 60°C for 20 s, 72°C for 30 s. The reference gene *D. citri Actin* (GenBank accession number: XM_008470467) was used as an internal control for normalisation, and the relative gene expression was calculated using the $2^{-\Delta\Delta Ct}$ method. A total of three biological replicates were performed for each treatment, and each biological replicate consisted of three technical replicates.

Statistical analysis

Experimental data from quantitative detection of *C*Las in the SG assay and RT-qPCR validation of DEGs were subjected to independent sample *t*-test using SPSS 25.0 software. Statistically significant differences were established as **P* < 0.05 or ***P* < 0.01.

Results

CLas infection in the SG of citrus psyllid

The SG samples were dissected in sterile PBS and then washed with DEPC-treated water to remove excess tissues. Thus, the detached SG showed relatively intact morphology (fig. 2). To verify the presence of *C*Las in the SG, PCR was performed using *C*Las-specific primer set OI1/OI2c with genomic DNA isolated from pooled *C*Las-infected SG samples. The results of gel electrophoresis showed that the *C*Las-infected SG exhibited clear OI1/

OI2c target fragments of 1167 bp in length, while that were not present in the control (fig. 3a). Meanwhile, the RT-qPCR test further validated the *C*Las infection in the SG of exposed ACP subcolony, which was consistent with the gel imaging results (fig. 3b). Overall, these results indicated that the selected SG samples could be used for the subsequent transcriptome sequencing.

Read assembly and Illumina sequencing

For quality assessment, fastp software was used to trim adaptor sequences and low-quality reads. In total, an average 6,686,101,700 and 6,680,688,100 raw reads from the SG of *C*Las-infected and uninfected ACP were generated, respectively. After data filtering, an average 6,568,553,270 and 6,565,561,078 high-quality clean reads were obtained with an average GC content of 44.18 and 44.35% (table 1). The mean Q20 (Phred score >20) and Q30 (Phred score >30) values were more than 96.8 and 91.4%, respectively. The paired-end clean reads were subsequently mapped to the ACP reference genome, which resulted in an average mapping rate of 80.26 and 80.12% from the two subcolonies (table 2). The results showed that the accuracy of the sequencing data was adequate for further analysis.

Quality control analyses of SG transcriptome samples

A correlation test was conducted to evaluate the reliability of two SG transcriptome samples from *C*Las-free and *C*Las-infected ACP as well as operational stability. The average Pearson's correlation coefficient R^2 values between transcriptome samples from *C*Las-free and *C*Las-infected ACP reached more than 99.69 and 99.68% (figs 4a and b), respectively, indicating that the SG transcriptome samples exhibited a high stability and repeatability.

In addition, the uncorrelated variable values converted from all transcriptome samples were subjected to PCA, and the total cumulative contribution rates of the first and second principal components to sample variance were 95.8% (fig. 4c), indicating that the quality of SG transcriptomes was adequately reliable. Accordingly, these results suggested that the correlation test and PCA were consistent with respect to the RNA-Seq datasets of *C*Las-infected and uninfected APC subcolonies.

Identification of DEGs

Significant differences in the SG of *C*Las-infected *D. citri* were founded compared with the uninfected *D. citri*. As a result, the comparative expression analysis resulted in a total of 25,624 genes in the SG transcriptomes of the two ACP subcolonies (table S2). Of these, 861 DEGs were identified in the *C*Las-infected ACP SG compared with the uninfected ACP, including 202 upregulated and 659 downregulated genes (fig. 5a, table S3). In addition, based on the transcript abundance of each sample, the hierarchical clustering analysis of all the DEGs was performed to evaluate the expression patterns of the identified genes (fig. 5b). These results suggested that *C*Las infection significantly altered the transcriptional profiles of the DEGs in the ACP SG.

GO and KEGG enrichment analysis of DEGs

GO enrichment analysis was performed to investigate the functions of the DEGs, and a corrected *P*-value <0.05 was defined as significant enrichment. In total, the GO assignments generated
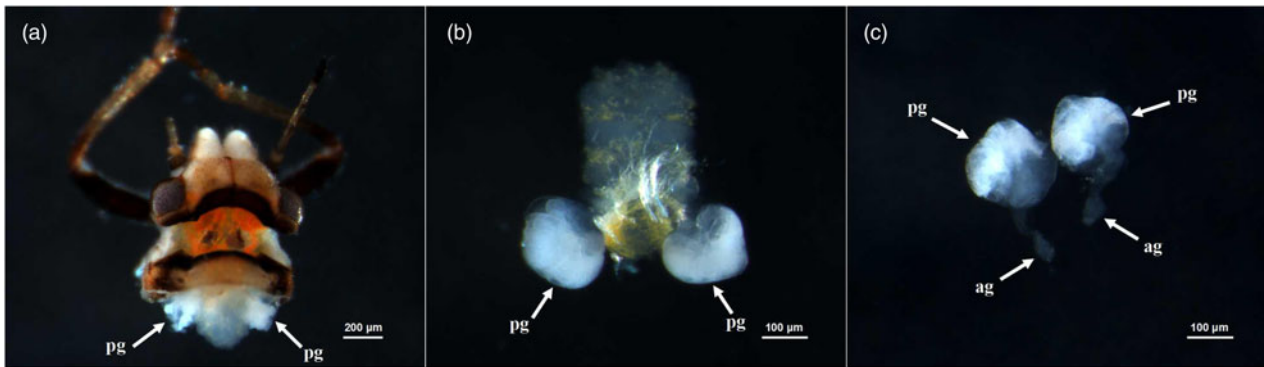
Figure 2. Morphology of the ACP SG that observed under a Discovery V20 stereomicroscope. (a) The position of the SG in the head of an ACP adult; (b) paired SG of an adult ACP; and (c) the structure of the whole excised ACP SG. pg, principal gland; ag, accessory gland.
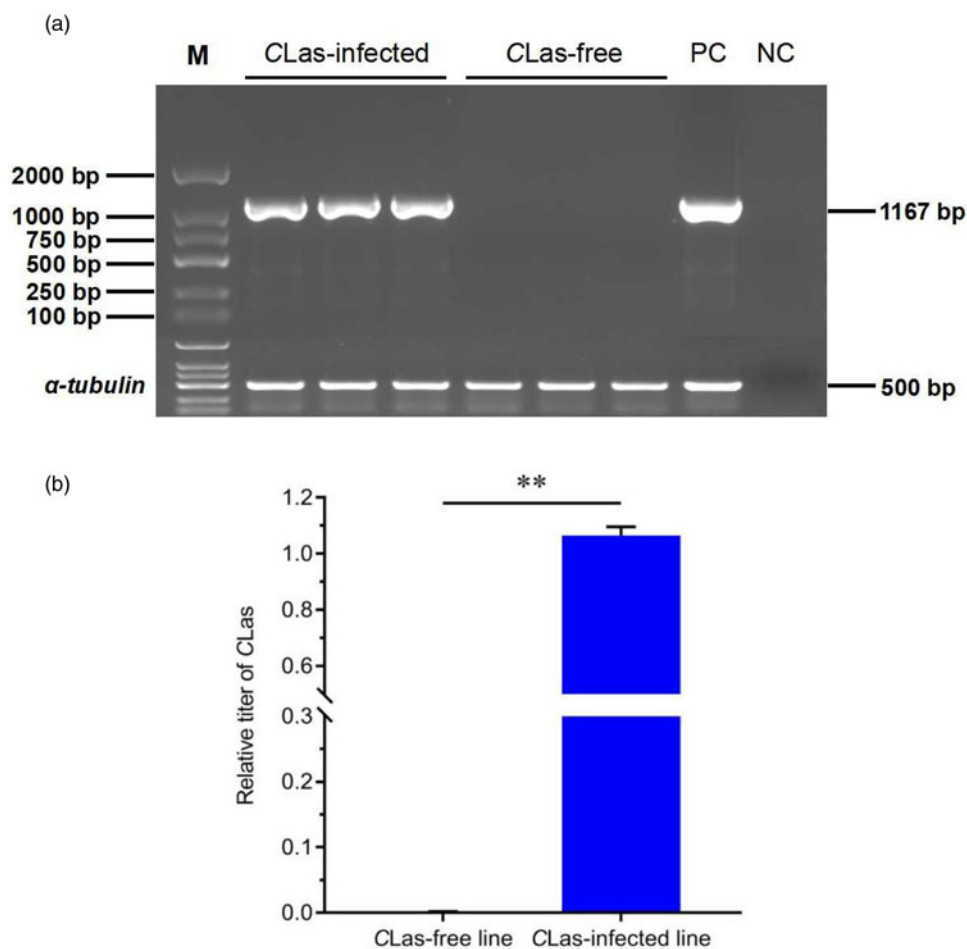

Figure 3. Qualitative and quantitative detection of *CLas* in the SG of *CLas*-free and *CLas*-infected citrus psyllid subcolonies. (a) Qualitative detection PCR. M, 2000 bp DNA marker; PC, positive control; NC, negative control. The *CLas*-exposed SG and ddH$_2$O were used as the DNA templates of positive control and negative control, respectively. *α*-tubulin: the reference gene for the presence of DNA template in each lane. (b) Quantitative detection RT-qPCR. The relative titre of *CLas* was calculated using the $2^{-\Delta\Delta Ct}$ method. The data represent mean ± SEM ($n = 3$), **$P < 0.01$ (independent *t*-test).

7516 GO terms, which were functionally grouped into three main categories: biological processes (5544 unigenes), cellular component (775 unigenes), and molecular function (1197 unigenes) (table S4). For each category, the top 20 most significantly enriched GO terms were selected for further analysis (fig. 6a, table S5). In biological processes, the majority of DEGs were associated with cellular processes, single-organism processes, and metabolic processes. A total of 52 upregulated DEGs were related to organic substance metabolic process, 44 upregulated DEGs were mainly involved in cellular metabolic process, and 40 upregulated DEGs were associated with nitrogen compound metabolic processes. In addition, a total of 46 DEGs were mainly

Table 1. Summary of data filtering statistics from two different treatments of citrus psyllid SG

Sample	CLas-Free_1	CLas-Free_2	CLas-Free_3	CLas-infected_1	CLas-infected_2	CLas-infected_3
Total raw reads	7,246,944,300	7,101,324,900	5,710,035,900	6,793,557,600	7,177,982,400	6,070,524,300
Total clean reads	7,110,804,748	6,978,542,133	5,616,312,930	6,681,104,690	7,055,910,270	5,959,668,274
GC (%)	43.83	44.48	44.23	44.47	44.28	44.29
Q20 (%)	96.40	96.85	97.15	96.81	96.91	96.73
Q30 (%)	90.59	91.51	92.10	91.43	91.68	91.27

involved in the immune system process, including 9 upregulated and 37 downregulated genes, indicating that CLas may suppress the host's immune responses by reducing the expression of immune-related genes. Among molecular function terms, binding, catalytic activity, and transporter activity were the most abundant of 13 categories, while in cellular component, the top three common categories were cell, cell part, and membrane. Among the top 20 assigned GO terms based on GO annotation, the DEGs were mostly enriched in GO functional categories of plasma membrane and cell periphery (fig. 6b, table S4). These results suggested that the cellular activities in *D. citri* SG were metabolically activated after CLas infection.

By assigning to the reference pathway in KEGG, the biological pathways affected by the DEGs were further analysed. According to the KEGG pathway classification, the DEGs were functionally grouped into 42 KEGG categories, including 276 pathways (fig. 7a, table S6). The top 20 KEGG-enriched pathways are shown in fig. 7b, and the majority of DEGs were predicted to be involved in mannose type *O*-glycan biosynthesis, oxytocin signalling pathway, peroxisome proliferator-activated receptor signalling pathway, and salivary secretion (table S7). Among these pathways, a total of eight, seven, three, and two DEGs were significantly enriched in endocytosis, lysosome, peroxisome, and phagosome, respectively. In addition, the enrichment analysis revealed the assignment of DEGs in multiple carbohydrate metabolism pathways, including pyruvate metabolism, glycolysis/gluconeogenesis, citrate cycle (TCA cycle), starch and sucrose metabolism, pentose and glucuronate interconversions, ascorbate and aldarate metabolism, amino sugar, and nucleotide sugar metabolism. Among amino acid metabolism pathways, arginine and proline metabolism, alanine, aspartate and glutamate metabolism, and cysteine and methionine metabolism were significantly altered. These results suggested that the SG were active in carbohydrate and amino acid metabolism, and the utilisation of these organics may be altered by CLas. Furthermore, several immune system-related pathways, like platelet activation, chemokine signalling pathway, nucleotide oligomerisation domain (NOD)-like receptor signalling pathway, and Toll and immune deficiency (Imd) signalling pathway were found to be significantly affected by the DEGs, indicating that CLas infection may modulate the immune defence in citrus psyllid SG.

RT-qPCR validation of DEGs

In order to verify the accuracy of the transcriptome sequencing data, the relative expression abundance of 16 DEGs (eight upregulated and eight downregulated genes) were randomly selected for RT-qPCR analysis (fig. 8a). All of the selective target genes are shown in table S8. A comparative analysis suggested that the RT-qPCR results were consistent with our RNA-Seq data

(fig. 8b). For instance, the genes of vitellogenin-2-like, acetylcholine receptor subunit alpha-like 1, and E3 ubiquitin-protein ligase MYCBP2-like in CLas-infected subcolony exhibited significant downregulation in both transcriptome data and the RT-qPCR analysis, with a similar fold change of expression level. Moreover, eight genes were upregulated in the SG after CLas infection, whereas only one gene (Adenosine triphosphate [ATP] dependent RNA helicase ddx17) had no significant change in the RT-qPCR analysis. In addition, we performed a linear regression analysis to determine the correlation between RT-qPCR and transcriptome data. The analysis resulted in a correlation coefficient R^2 value of 0.9408 and a corresponding slope of 0.8227 (fig. 8c), indicating a significant correlation between RT-qPCR and the transcriptome data. In summary, these results confirmed the reliability of the RNA-Seq data.

Analysis of DEGs associated with ubiquitination, cytoskeleton, and salivary secretion

Based on functional annotation, the DEGs involved in ubiquitination, cytoskeleton, and salivary secretion showed significant differences in the SG transcriptome between CLas-free and CLas-infected ACP subcolonies (fig. 9, table 3). In the present study, a total of 12 ubiquitination-related DEGs were obtained from the SG transcriptome. Among them, ten DEGs were downregulated in the SG after CLas infection, while two DEGs associated with ubiquitin mediated proteolysis were upregulated, including RING-box protein HRT1-like and cullin-2. For cytoskeleton analysis, a total of 15 DEGs were identified, and 13 DEGs were significantly downregulated, except for troponin T-like and troponin T isoform X11. In addition, we also observed decreased levels of DEGs involved in salivary secretion in the CLas-infected *D. citri* SG transcriptome compared with that in the control. These results revealed that infection with CLas led to lower levels of DEGs involved in ubiquitination, the cytoskeleton, and salivary secretion in ACP SG, which may be important in the process of CLas invasion.

Analysis of DEGs associated with endocytosis, lysosome, and xenobiotics biodegradation and metabolism

According to the GO and KEGG enrichment analyses, many DEGs were classified and significantly enriched in endocytosis, lysosome, and xenobiotics biodegradation and metabolism (fig. 10, table 4). In this instance, a total of 21 DEGs related to endocytosis were found to be significantly downregulated in CLas-infected ACP subcolony. For the lysosome analysis, seven DEGs exhibited significant downregulation in the SG under CLas infection, including four upregulated DEGs and three downregulated DEGs. For xenobiotics biodegradation and metabolism,

Table 2. Statistics of the number of reads and their ratios mapped to citrus psyllid reference genome in the two SG transcriptomes

Sample	CLas-Free_1	CLas-Free_2	CLas-Free_3	CLas-infected_1	CLas-infected_2	CLas-infected_3
Total	47,185,226	46,506,390	37,351,498	44,503,916	46,758,538	39,627,012
Total mapped (%)	37,596,732 (79.68%)	37,322,874 (80.25%)	30,203,869 (80.86%)	35,748,151 (80.33%)	37,450,636 (80.09%)	31,672,930 (79.93%)
Unmapped (%)	9,588,494 (20.32%)	9,183,516 (19.75%)	7,147,629 (19.14%)	8,755,765 (19.67%)	9,307,902 (19.91%)	7,954,082 (20.07%)
Unique_mapped (%)	29,094,535 (61.66%)	28,895,805 (62.13%)	23,300,445 (62.38%)	27,458,313 (61.70%)	29,276,477 (62.61%)	24,569,113 (62.00%)
Multiple_mapped (%)	8,502,197 (18.02%)	8,427,069 (18.12%)	6,903,424 (18.48%)	8,289,838 (18.63%)	8,174,159 (17.48%)	7,103,817 (17.93%)

a total of 12 DEGs showed significant changes; of these DEGs, five genes were significantly upregulated and seven genes were significantly downregulated in *C*Las-infected *D. citri* compared with the uninfected control. These results indicated that the endocytosis, lysosome, and xenobiotics biodegradation and metabolism may play crucial roles in the SG response to *C*Las infection.

Discussion

D. citri is currently the principal transmission vector of *C*Las bacterium that causes the destructive citrus greening disease (HLB) worldwide. The SG is an important secretory tissue in *D. citri* with functions in insect feeding, resisting against pathogens, and overcoming plant defences, and it also acts as a barrier to the transmission of *C*Las (Giron *et al.*, 2016). However, the molecular mechanism of SG defence against *C*Las infection remains unclear. Recent findings have uncovered the transcriptomic and proteomic differences between *C*Las-infected and uninfected *D. citri* involving the cytoskeleton, ubiquitination, metabolism, insecticide resistance, and immune system (Kruse *et al.*, 2017, 2018; Yu *et al.*, 2020; Liu *et al.*, 2021). In the current study, we focused on the transcription level changes of the SG conferred by *C*Las infection in *D. citri* by using a comparative transcriptomic approach. The transcriptome dataset revealed the functional annotation of DEGs involved in the lysosome, endocytosis, cellular processes, metabolic processes, the immune system, and digestion system. These results suggested that the HLB pathogen may manipulate multiple essential biological processes in host vector to promote its transmission and proliferation.

In host–pathogen interactions, many pathogens interact with highly conserved host components for extracellular recognition and attachment, such as cytoskeleton. The cytoskeleton is a major host structural component, which is essential for controlling cell shape, adhesion, migration, and intracellular transport (Wen *et al.*, 2020; Benoit *et al.*, 2021). The bacterial pathogens modulate the host cytoskeleton to thrive and promote numerous infection events, including invasion, intracellular replication, and dissemination (Colonne *et al.*, 2016). Sarkar *et al.* revealed that the vector-borne 'Candidatus Liberibacter solanacearum' employed the actin cytoskeleton of gut cells for successful movement and transmission in the host vector (Sarkar *et al.*, 2021). Moreover, several *Liberibacter* species inducing cytoskeletal rearrangements of host cell for invasion and systemic infection in psyllids have also been reported (Ghosh *et al.*, 2019; Tang and Tamborindeguy, 2020). In the current study, many DEGs were mostly enriched in the pathway of regulation of actin cytoskeleton. In addition, a total of 15 DEGs associated with the cytoskeleton were identified, and most were significantly downregulated in the *C*Las-infected groups compared with uninfected groups. For example, actin and tubulin, the major protein constituents of cytoskeletal filaments involved in cell motility and signal transduction (Gouin *et al.*, 2005), were significantly downregulated after *C*Las infection. Rap proteins belong to small GTPases involved in cellular signal transduction, adhesion, and the regulation of cytoskeletal dynamics. Interestingly, the Rap 1 signalling pathway, which involves the metabolism of talin, integrin, actin, and other cytoskeletal proteins (Bromberger *et al.*, 2019; Maywald *et al.*, 2022), was significantly assigned to the top 20 pathways in KEGG (fig. 7). Furthermore, a previous study had revealed the disrupted architecture of actin cytoskeleton within the *D. citri* midgut following exposure to *C*Las (Ghanim *et al.*, 2016). This may result from the reduced expression of
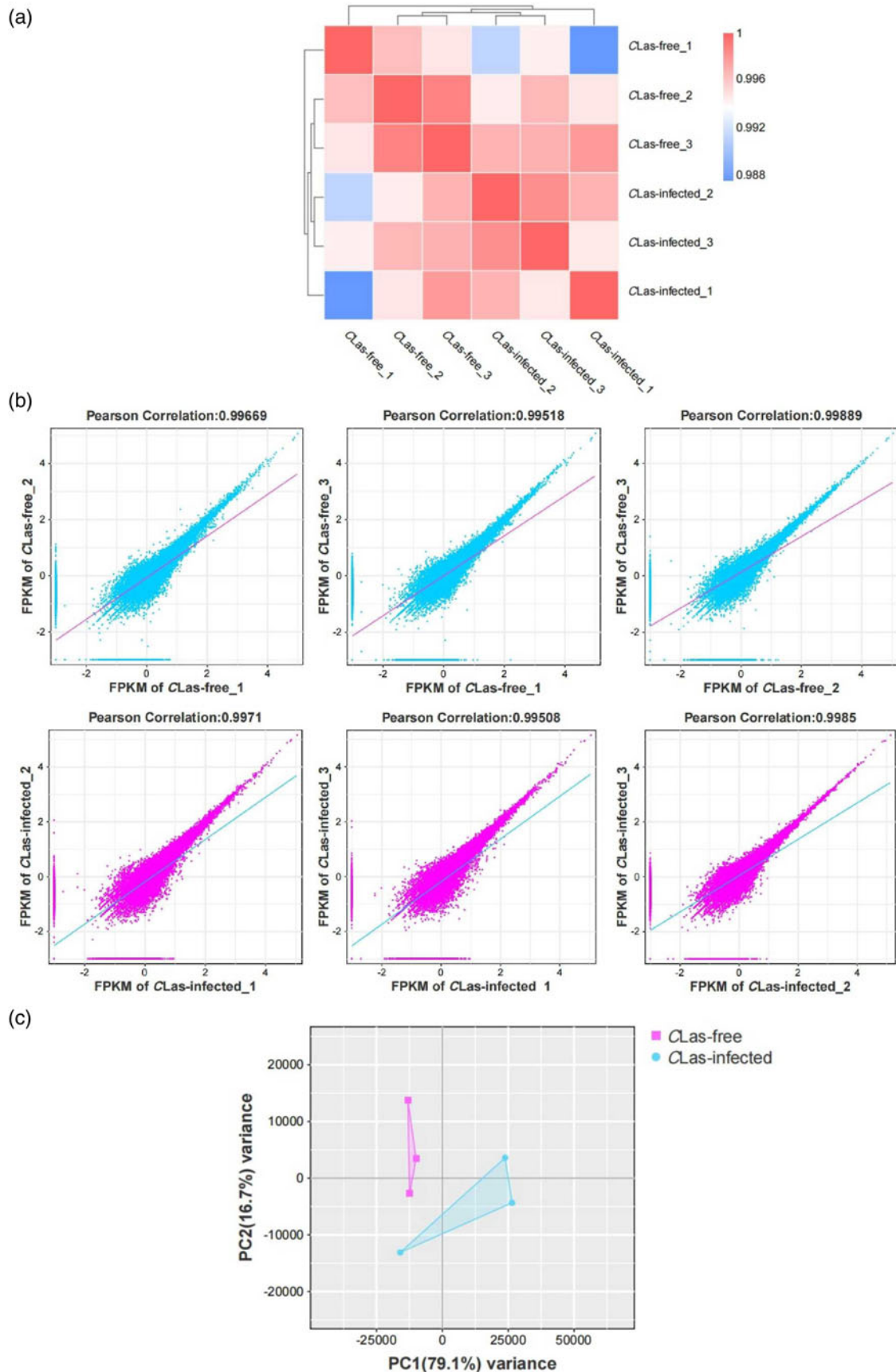
(a)

(b)

(c)

Figure 4. Relationship analyses of the SG transcriptome samples from *C*Las-free and *C*Las-infected ACP. The repeatability and diversity of the SG transcriptome samples were calculated according to correlation heat map (a), scatter plots, (b) and PCA (c). The oblique line represents the fitting line of the scatter distribution. The Pearson's correlation coefficient was calculated based on the FPKM value of each sample.
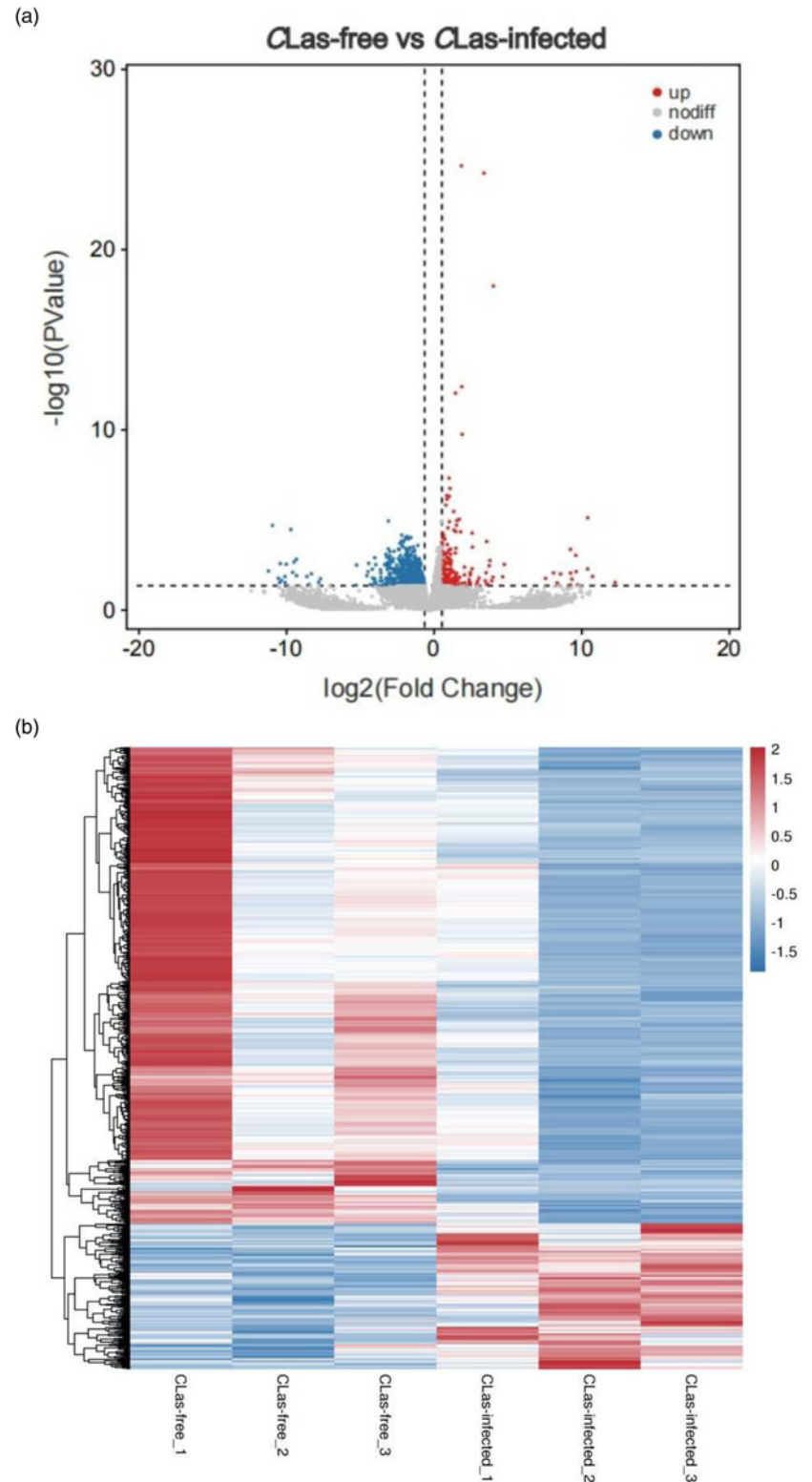
(a)

(b)

Figure 5. Identification and hierarchical cluster analysis of DEGs between *C*Las-free and *C*Las-infected ACP. (a) Volcano plot for the expression pattern of each gene. The abscissa represents the fold change of gene expression in different samples, and the ordinate indicates the significance level of difference in DEGs. The red, blue, and grey points represent upregulated, downregulated, and no significant difference genes, respectively. (b) Hierarchical clustering of DEGs. Rows represent different DEGs, and columns indicate different samples. Red bands and blue bands indicate high and low gene expression level, respectively.

cytoskeleton-related proteins induced by the *C*Las infection. Remarkably, vitellogenin transcription was also responsive to *C*Las-infection in the SG because of its involvement in host recognition (table S3). Vitellogenin is one of the major known pattern recognition receptors with functions in insect fecundity and eliciting host immunity (Han *et al.*, 2022; Sarkar and Ghanim, 2022). It often acts as a pattern recognition molecule to recognise

pathogens, enhance macrophage phagocytosis and autophagy (Brumin *et al.*, 2020; Sarkar and Ghanim, 2022). Previous reports have showed that *C*Las infection causes the upregulation of vitellogenin genes in the haemolymph, gut, and whole body of *D. citri* (Ramsey *et al.*, 2017; Kruse *et al.*, 2018; Liu *et al.*, 2021). However, the majority of vitellogenin genes were unexpectedly downregulated in the SG conferred by *C*Las, indicating that
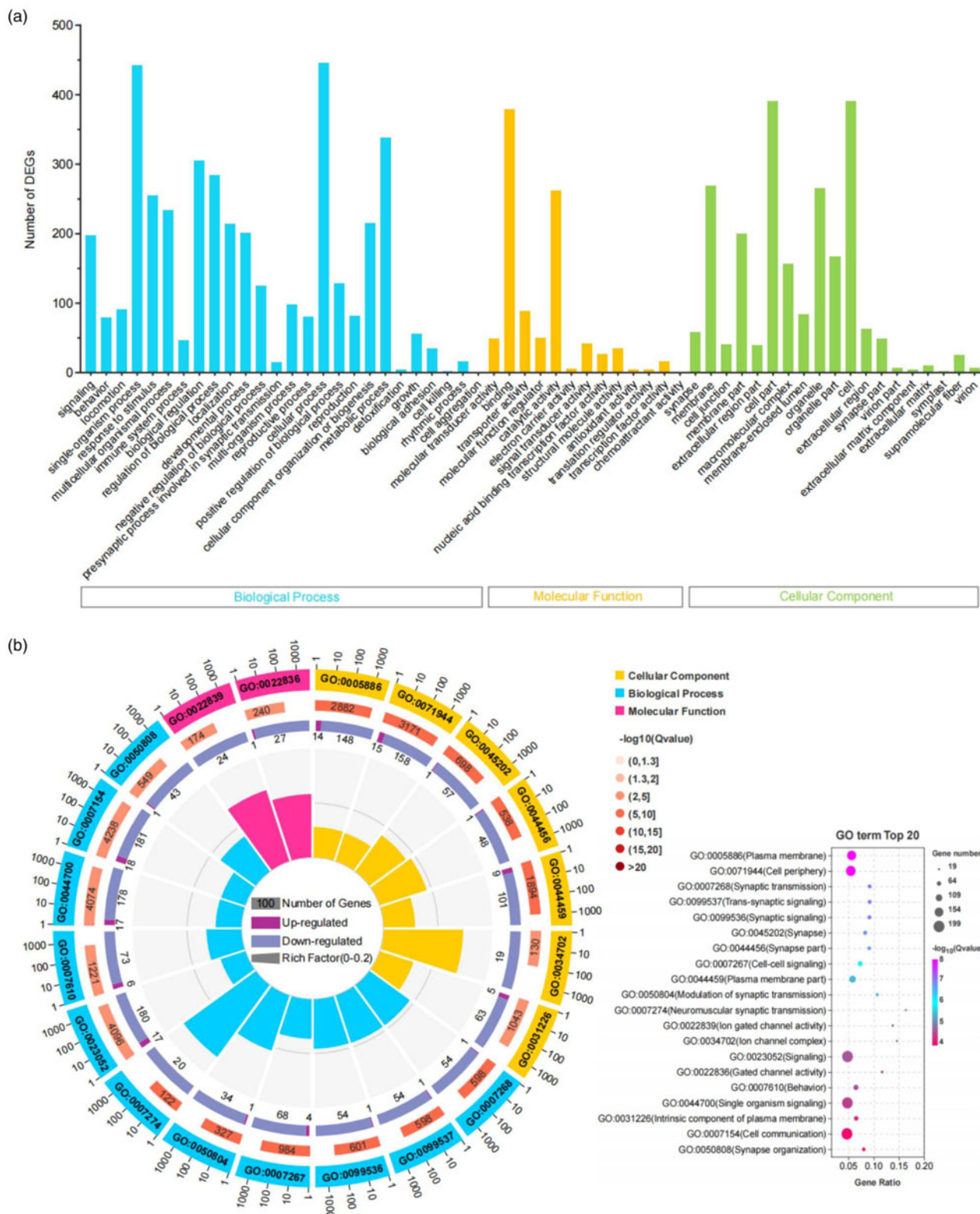
Figure 6. GO classification and enrichment analysis of DEGs between CLas-free and CLas-infected ACP. (a) Statistics of the enriched GO terms and genes in GO database according to hierarchical classification. The abscissa represents three main functional categories: BP, biological process; CC, cellular component; and MF, molecular function. For each category, the top 20 GO terms were selected for functional analysis. The ordinate indicates the number of DEGs. (b) GO enrichment analysis of DEGs. The outer ring represents the enriched top 20 GO terms, and different colours indicate different ontologies. Ring 2 represents the gene counts and Q-value in the corresponding GO terms background. The bar length represents the number of DEGs, and the colour changes represent the various Q-values. Ring 3 represents the counts for upregulated and downregulated genes in the corresponding GO terms. The inner ring represents the rich factor values (the number of DEGs divided by the number of background genes in the corresponding GO terms). Each cell in the background grid lines represents 0.1. The scatter diagram of top 20 enriched GO categories. The abscissa indicates the gene ratio. The ordinate indicates different categories.
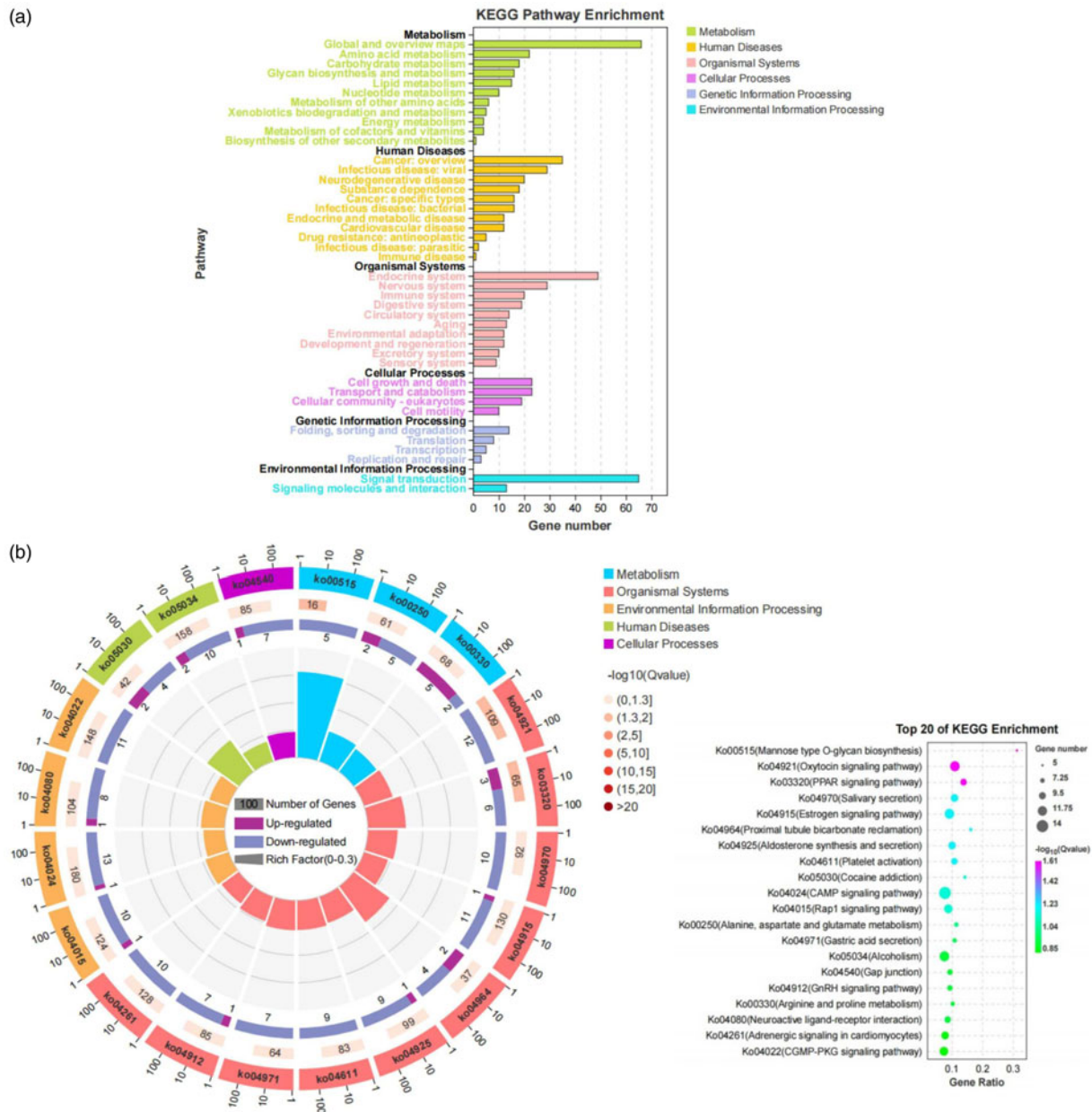
(a)

(b)

Figure 7. KEGG classification and enrichment analysis of DEGs. (a) Statistics of the enriched pathways and genes in KEGG database based on hierarchical classification. The *X*-axis indicates the number of DEGs. The *Y*-axis indicates different pathways. (b) KEGG enrichment analysis of DEGs. The outer ring indicates the enriched top 20 pathways, and different colours indicate different clusters. Ring 2 indicates the pathway counts and *Q*-value in the corresponding DEG background. The bar length represents the number of DEGs, and the colour changes represent the various *Q*-values. Ring 3 indicates the counts for upregulated and downregulated DEGs in the corresponding pathway. The inner ring indicates the rich factor values (the number of DEGs divided by the number of background genes in the corresponding pathway). Each cell in the background grid lines represents 0.1. The scatter diagram of top 20 enriched KEGG pathways. The *X*-axis indicates the gene ratio and the *Y*-axis indicates different categories.

*C*Las may induce low expression of vitellogenin genes for successful evasion and proliferation. This result is consistent with a previous study that showed the reduced vitellogenin in *C*Las-infected *D. citri* (Vyas *et al*., 2015), and our hypothesis contributes to explaining the potential upregulation of the *C*Las titre by silencing of a vitellogenin-like protein in *D. citri* (Peng *et al*., 2023). In general, our findings suggested that *C*Las might inhibit the expression of cytoskeleton-associated proteins and vitellogenin genes in the SG to avoid the host immune recognition and facilitate its transmission.

The replication and circulation of the HLB pathogen in SG depend on the suppression of host immune defence and overcoming the SG barrier. The bacterium possibly manipulates the vector host ACP directly and/or indirectly to enhance its spread and transmission (Galdeano *et al*., 2020), and the immune defence mechanism of SG in response to *C*Las invasion remains unclear. In this instance, many DEGs are significantly enriched in pathways involved in immune defences, such as the NOD-like receptor signalling pathway, ubiquitin-mediated proteolysis, and Toll and Imd signalling pathway. Among these pathways, numerous immune-related genes, like heat shock proteins, serine/threonine-protein kinases, cathepsins, ubiquitin-ligases, and so forth, were significantly altered in the *C*Las-infected SG.
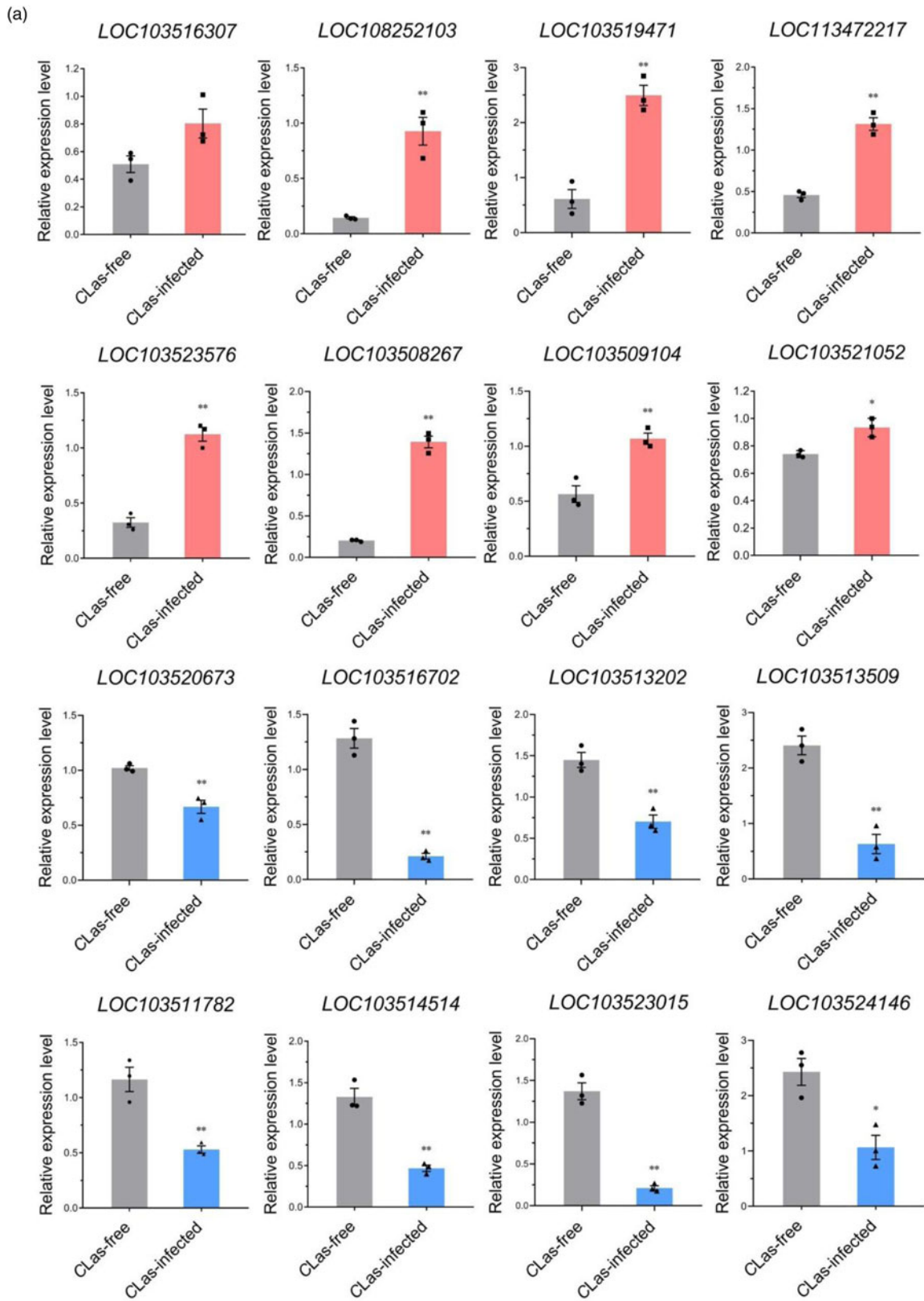
Figure 8. Correlation analysis of the RNA-Seq data and RT-qPCR validation. (a) The relative transcription abundance of 16 DEGs from the SG transcriptomes between CLas-free and CLas-infected ACP. The relative expression levels were calculated using the $2^{-\Delta\Delta Ct}$ method, and the significant differences are indicated by *$P < 0.05$ or **$P < 0.01$ using independent t-test. (b) Comparison of the transcriptome data and RT-qPCR results. The data represent mean ± SEM ($n = 3$). (c) The linear regression analysis between the transcriptome and RT-qPCR data. The abscissa indicates the ratios obtained by RT-qPCR, and the ordinate indicates the ratios obtained by RNA-Seq.
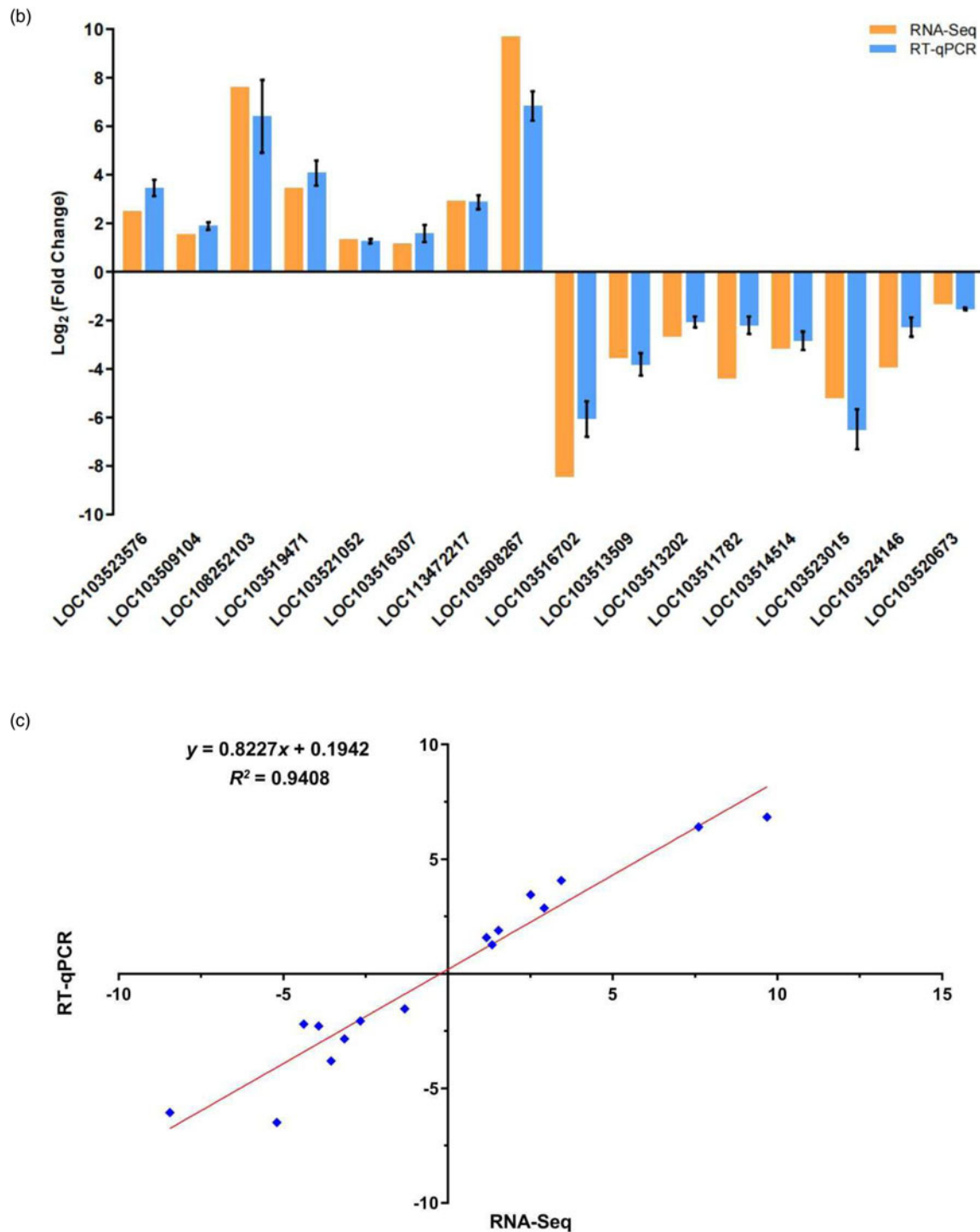
(b)

(c)

Figure 8. Continued.

Cathepsins belong to the papain-like family of cysteine proteases involved in various physiological processes, including apoptosis, intracellular protein degradation, and the immune response (Yang *et al.*, 2020; Chen *et al.*, 2023). For example, Sun *et al.* revealed that cathepsins O and L may be involved in the innate immune system of *Antheraea pernyi* Guer (Sun *et al.*, 2018, 2017); Guo *et al.* revealed a novel function for a cathepsin-type protease cathepsin B3 in aphid saliva that elicited effective host plant defences in phloem (Guo *et al.*, 2020); Yu *et al.* identified two *D. citri* cathepsin genes induced by *C*Las, indicating their potential roles in the innate immune response (Yu *et al.*, 2019). In this study, a total of 37 cathepsin genes were identified in the SG, and one cathepsin L-like gene was significantly downregulated in *C*Las-infected ACP. Our result suggested that cathepsins may be important in the SG defence against *C*Las invasion. For the immune response analysis, we also observed that many DEGs associated with ubiquitination pathway were altered in the obtained SG transcriptome. Ubiquitination is an enzymatic
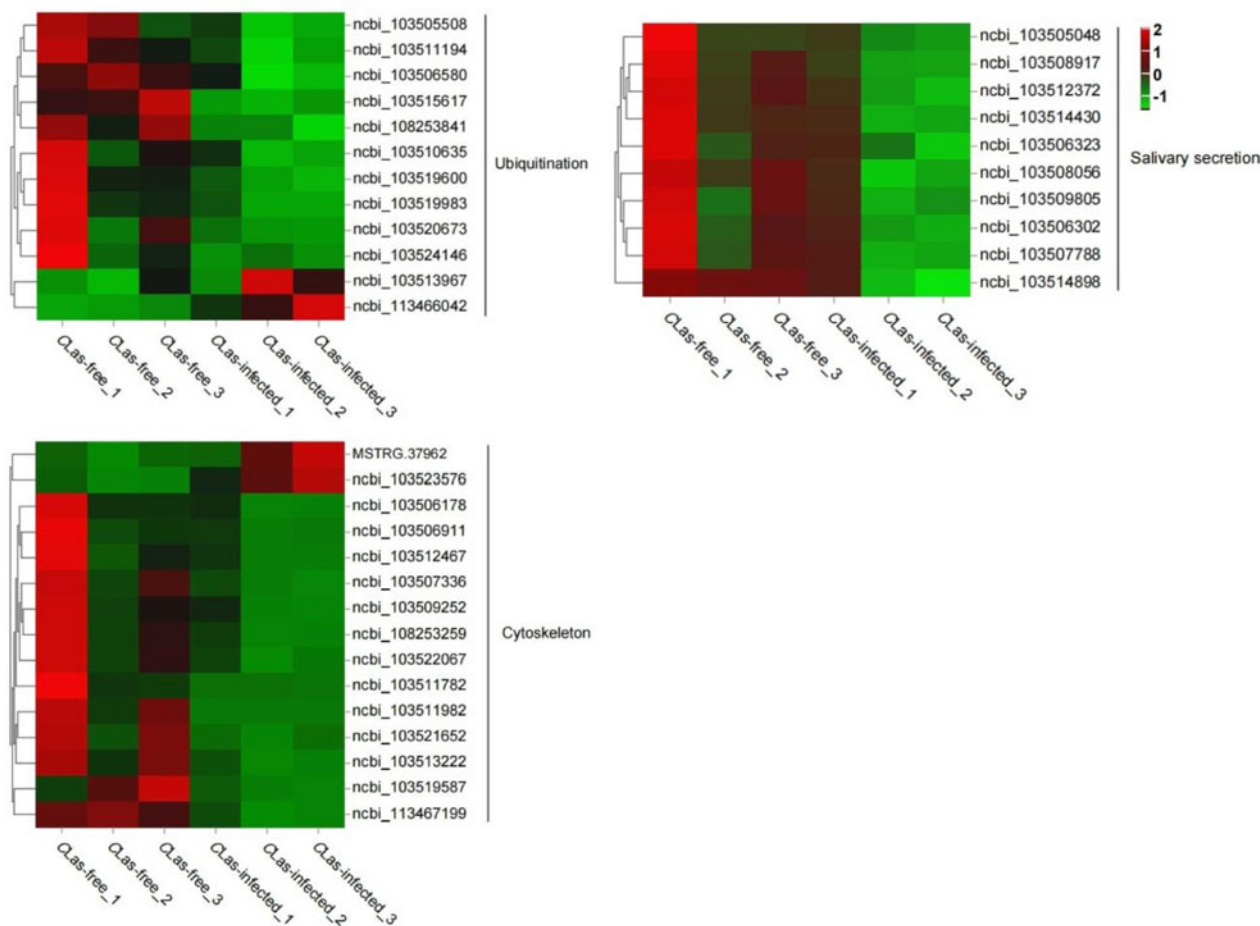
Figure 9. Hierarchical cluster analysis of DEGs involved in ubiquitination, cytoskeleton, and salivary secretion between *C*Las-free and *C*Las-infected ACP SG. Red colour indicates high gene expression level, and green colour indicates low gene expression level.

cascade reaction catalysed by several classes of enzymes, including ub-activating enzyme E1, ub-conjugating enzymes E2, and ub-protein ligase E3 (Swatek and Komander, 2016). Ubiquitination involves membrane trafficking and endocytosis, and it plays critical roles in bacterial recognition, targeting, and clearance (Grumati and Dikic, 2018; Mukherjee and Dikic, 2022). Furthermore, the ubiquitin proteasome system also acts as a key signalling pathway in the host immune response to infection (Ligeon *et al.*, 2011). In this study, we identified 12 ubiquitination-related DEGs in the SG transcriptome. Of those genes, ten DEGs were significantly downregulated after *C*Las infection, including five E3 ubiquitin-protein ligase genes. Yu *et al.* also identified 13 DEGs involved in ubiquitination in the *D. citri* midgut after exposure to *C*Las (Yu *et al.*, 2020). Thus, ubiquitination-correlated genes might play an important role in the process of *C*Las infection. Moreover, previous studies have revealed that many bacterial effectors enable them to interfere with the ubiquitination pathway to avoid triggering the immune responses (Munro *et al.*, 2007; Spallek *et al.*, 2009). Overall, we considered that *C*Las may suppress cathepsins and host ubiquitination process to reduce immune-related proteins in the SG of *D. citri*.

The *C*Las bacterium is an obligate intracellular pathogen with a relatively small genome (Duan *et al.*, 2009). Comparative genome sequencing of *C*Las with the closest cultured relative revealed that *C*Las is not able to synthesise several essential elements, such as the aromatic amino acids, fatty acids, vitamins, and lipopolysaccharides (Lai *et al.*, 2016). Consequently, *C*Las needs to rely on the insect vector for these essential nutrients. Based on KEGG enrichment analysis, the significant changes conferred by *C*Las infection were with respect to the pathways involved in nutrient and detoxification metabolism. Trehalose is the major non-reducing circulatory disaccharide in the haemolymph of insects, and provides instant energy substance and defence against abiotic stresses (Iordachescu and Imai, 2008; Shukla *et al.*, 2015). Trehalase, a hydrolase that catalyses a trehalose molecule into two glucose molecules, is synthesised in the fat body and then transported to the haemolymph via trehalose transporter (Wang *et al.*, 2021). It has been well documented that insect trehalase can regulate numerous biological processes and metabolic pathways involved in insect homoeostasis, flight, growth, development, nutrition, energy metabolism, and chitin synthesis during moulting (Zhao *et al.*, 2016; Yasugi *et al.*, 2017). In our study, seven trehalase genes were identified in SG transcriptome (table 5), and the induced expression of trehalases post-*C*Las exposure indicated that *C*Las may regulate trehalose metabolism pathway by stimulating trehalase activity for nutrition availability. The transcriptomic results also suggested that *C*Las modulated the detoxification metabolism in *D. citri* SG. Insect detoxification enzymes, such as cytochrome P450 monooxygenases (*CYPs*), UDP-glycosyltransferases (*UGTs*), and glutathione *S*-transferases

Table 3. Presence of the DEGs upon *C*Las infection involved in ubiquitination, cytoskeleton, and salivary secretion between *C*Las-free and *C*Las-infected *D. citri* SG transcriptome

| Gene ID	*C*Las-free_FPKM	*C*Las-infected_FPKM	log 2 (FoldChange)	Gene description
Ubiquitination				
ncbi_103515617	2.720	1.355	−1.004958937	E3 ubiquitin-protein ligase Bre1-like
ncbi_103505508	5.722	2.849	−1.006063876	E3 ubiquitin-protein ligase Bre1-like
ncbi_108253841	13.293	6.598	−1.010602226	Ubiquitin fusion degradation protein 1 homologue
ncbi_103510635	1.889	0.906	−1.060294302	Apoptosis-resistant E3 ubiquitin protein ligase 1
ncbi_103519983	6.540	2.787	−1.23050410	Ubiquitin-associated domain-containing protein 1, partial
ncbi_103520673	0.887	0.356	−1.315706657	E3 ubiquitin-protein ligase MYCBP2-like
ncbi_103524146	0.816	0.0537	−3.926470965	E3 ubiquitin-protein ligase PPP1R11-like isoform X1
ncbi_103506580	7.834	3.405	−1.201891717	Uncharacterised protein LOC103506580 isoform X1
ncbi_103513967	3.463	5.606	0.694949357	RING-box protein HRT1-like
ncbi_103511194	17.287	10.018	−0.7870171860	Deubiquitinase DESI2 isoform X1
ncbi_103519600	3.1567	0.794	−1.990585474	Anaphase-promoting complex subunit 7-like
ncbi_113466042	0.0687	0.952	3.793279737	Cullin-2
Cytoskeleton				
ncbi_103523576	0.255	1.452	2.507918816	Troponin T-like
MSTRG.37962	3.690	7.552	1.03310763	Troponin T isoform X11
ncbi_103511782	1.173	0.056	−4.380070362	Tyrosine-protein kinase RYK-like
ncbi_108253259	1.914	0.442	−2.114472555	Class II receptor tyrosine kinase-like, partial
ncbi_103509252	13.598	5.789	−1.231889979	ALK tyrosine kinase receptor isoform X1
ncbi_103507336	1.5297	0.681	−1.168196941	Gamma-tubulin complex component 3 homologue
ncbi_103506911	3.061	1.118	−1.453513062	Myosin-VIIa, partial
ncbi_103519587	0.9617	0.221	−2.123668197	Unconventional myosin-XV-like
ncbi_103506178	13.803	7.828	−0.818204769	Kinesin light chain
ncbi_103521652	2.6537	1.025	−1.372363252	Kinesin-like protein Klp10A
ncbi_103522067	7.842	2.335	−1.747593154	Kinesin-like protein unc-104, partial
ncbi_103512467	0.711	0.199	−1.833990049	Kinesin-like protein GA13060
ncbi_103513222	10.336	2.561	−2.01304008	Kinesin-like protein unc-104
ncbi_103511982	1.903	0.001	−10.89431253	Kinesin-like protein KIF3B
ncbi_113467199	16.861	7.532	−1.162620525	Actin-1-like
Salivary secretion				
ncbi_103505048	7.383	2.335	−1.660643806	Calmodulin-like
ncbi_103506302	1.455	0.451	−1.689489262	Head-specific guanylate cyclase
ncbi_103506323	6.657	3.486	−0.933365315	Guanylate cyclase soluble subunit beta-1
ncbi_103507788	5.117	1.537	−1.734962199	Sodium/potassium-transporting ATPase subunit alpha
ncbi_103508056	3.379	1.6213	−1.059415622	1-phosphatidylinositol 4,5-bisphosphate phosphodiesterase classes I and II-like
ncbi_103508917	26.409	6.137	−2.105424185	Vesicle-associated membrane protein 2
ncbi_103509805	4.906	1.593	−1.622499116	Caltractin ICL1a-like
ncbi_103512372	5.643	1.722	−1.712741719	Calcium-activated potassium channel slowpoke-like
ncbi_103514430	101.913	38.086	−1.420005412	Sodium/potassium-transporting ATPase subunit beta-2-like isoform X5
ncbi_103514898	15.516	9.635	−0.687431103	Adenylate cyclase type 3-like
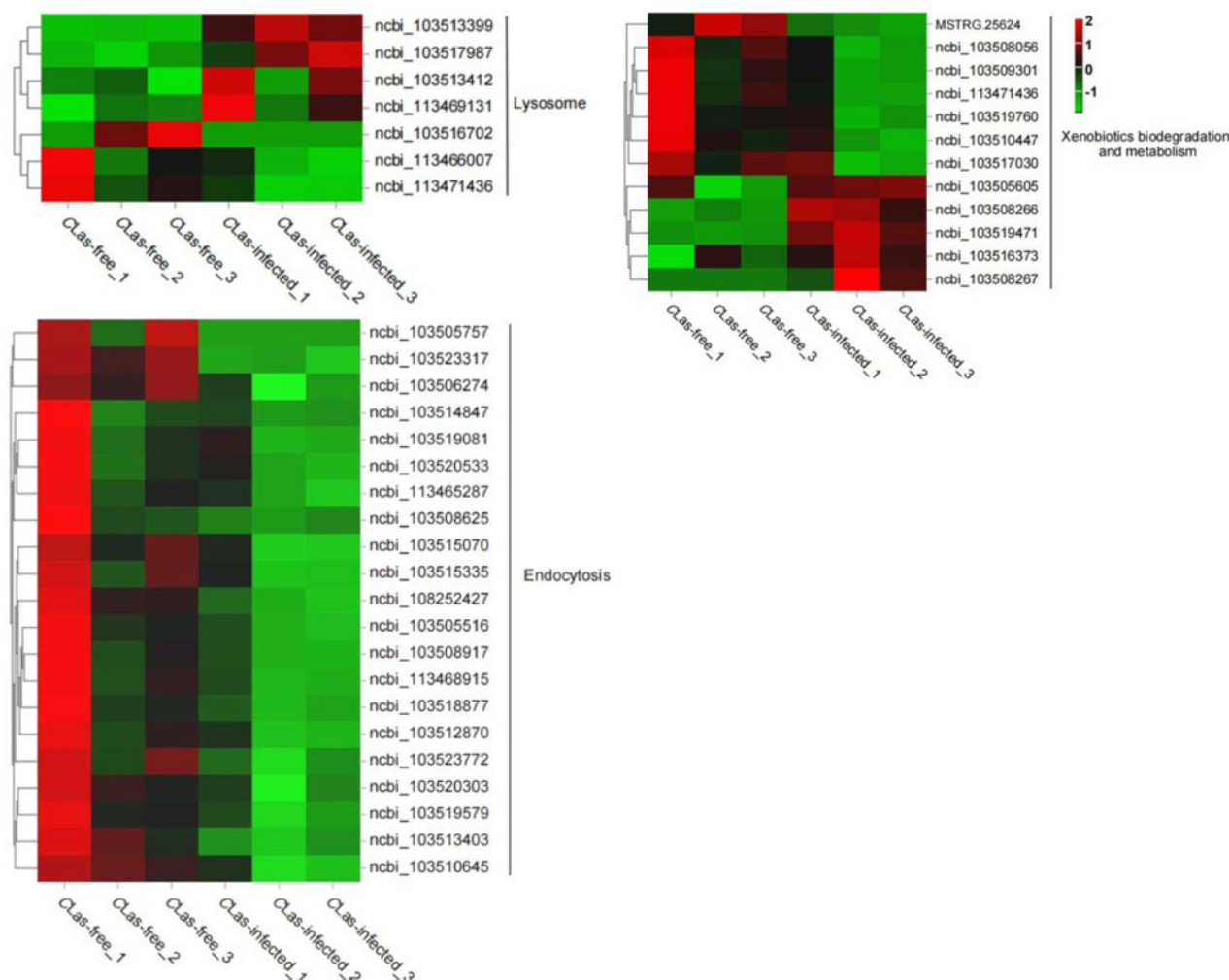
Figure 10. Hierarchical cluster analysis of DEGs associated with endocytosis, lysosome, and xenobiotics biodegradation and metabolism between CLas-free and CLas-infected ACP SG. Red colour represents high gene expression level, and green colour represents low gene expression level.

(*GSTs*), are well known to be involved in metabolic detoxification of xenobiotics (Lu *et al.*, 2021; Gao *et al.*, 2022). *CYP*s and *GST*s have been well documented in the SG of several hemipteran insects. For instance, 41 *CYP*s and 4 *GST*s were predicted in the SG of *E. fabae* (DeLay *et al.*, 2012), and 59 *CYP*s and 20 *GST*s genes were found with various expression levels in *Nephotettix cincticeps* Uhler (Matsumoto *et al.*, 2014). Su *et al.* identified eight *CYP*s and five *GST*s genes in SG transcriptome of *B. tabaci*, and a number of genes involved in metabolism and transport were significantly enriched (Su *et al.*, 2012). Ji *et al.* also performed transcriptomic analyses of two *N. lugens* populations with different virulence; in total, nine and ten *GST* genes were obtained from the SG, respectively (Ji *et al.*, 2013). Moreover, 14 *CYP*s genes (including nine genes upregulated and five genes downregulated) were found to be differentially expressed between the brown planthopper (BPH) populations, and genes related to metabolism, binding, and transport were significantly active. In our DEGs, a total of 21 *GST* genes were identified in the SG transcriptome. Two *CYP* genes and two *UGT* genes were significantly upregulated after *C*Las infection. Other detoxification enzymes, like esterases (*EST*s), were also considered to be responsible for the metabolism of xenobiotics in insects (Xu *et al.*, 2021). Five *EST* genes were significantly downregulated in the SG of

*C*Las-infected *D. citri*. These results are in accordance with previous reports that showed the altered detoxification-related genes in *C*Las-positive *D. citri* (Tiwari *et al.*, 2011; Kruse *et al.*, 2017). In conclusion, our observations suggested that *C*Las may manipulate trehalase activities and the transcription of detoxification enzymes during infection to facilitate its proliferation in the SG.

The transmission of *C*Las involves the propagation and circulation of the bacterium within host vectors, and the pathogen may alter the fitness, survival, and behaviour of its insect host. Previous study reported that the *C*Las-infected psyllids showed a significant reduction in total non-probing time, salivation time, and phloem ingestion time, indicating that *D. citri* were at a higher hunger level and they tended to forage more often after *C*Las infection (Killiny *et al.*, 2017). During psyllids feeding, salivary secretions play crucial roles in tissue penetration, lubrication, digestion, and nutrient ingestion. Mucin-like proteins (Mul) are a group of glycoproteins that cover the epithelial cell layer of many cuticle-free tissues in insects, such as the SG, midgut and Malpighian tubules (Lou *et al.*, 2019; Zhao *et al.*, 2020; Ahmed *et al.*, 2021). Mul are abundantly secreted as the principal components of saliva during insect feeding, and specifically expressed in the SG. In the transcriptome herein obtained, we identified 59 mucin-like proteins from dissected ACP SG, and the most

Table 4. Presence of the DEGs upon CLas infection involved in endocytosis, lysosome, and xenobiotics biodegradation and metabolism between CLas-free and CLas-infected *D. citri* SG transcriptome

Gene ID	CLas-free_FPKM	CLas-infected_FPKM	log 2 (FoldChange)	Gene description
Endocytosis				
ncbi_103519579	53.015	31.776	−0.73844795	Heat shock protein 83-like
ncbi_103508625	0.823	0.0703	−3.548611932	Vesicular acetylcholine transporter-like
ncbi_108252427	22.032	12.788	−0.784787988	Adenosine diphosphate (ADP) ribosylation factor-like protein 8B-A
ncbi_103519081	7.943	3.440	−1.207475784	Nicotinamide adenine dinucleotide phosphate (NADP) dependent malic enzyme-like
ncbi_103508917	26.409	6.137	−2.105424185	Vesicle-associated membrane protein 2
ncbi_103520533	8.461	4.085	−1.050374388	Synaptic vesicle membrane protein VAT-1 homologue-like
ncbi_113465287	3.989	1.640	−1.282210747	Synaptic vesicle membrane protein VAT-1 homologue-like
ncbi_103512870	98.480	49.888	−0.981137929	Synaptotagmin 1
ncbi_103514847	0.517	0.107	−2.268066093	Uncharacterised protein LOC103514847
ncbi_103515335	18.304	8.630	−1.084782218	Excitatory amino acid transporter isoform X1
ncbi_113468915	44.434	17.458	−1.347786551	Synaptotagmin 1-like
ncbi_103523317	3.162	1.087	−1.540043086	BET1 homologue
ncbi_103505516	11.576	5.470	−1.081477718	Folate receptor gamma-like isoform X1
ncbi_103523772	61.242	37.373	−0.712504302	Heat shock protein 83-like
ncbi_103505757	1.317	0.001	−10.36303963	Coiled-coil domain-containing protein 97-like
ncbi_103506274	0.703	0.300	−1.228562189	Epidermal growth factor receptor
ncbi_103510645	3.263	1.738	−0.908770905	Centaurin-gamma-1A
ncbi_103513403	19.244	11.558	−0.735475323	Charged multivesicular body protein 7
ncbi_103515070	11.112	5.853	−0.924913597	Atypical protein kinase C
ncbi_103518877	2.419	0.799	−1.597541611	Serine/arginine repetitive matrix protein 1
ncbi_103520303	41.275	25.491	−0.695287459	Ras-like GTP-binding protein Rho1
Lysosome				
ncbi_103513399	9.705	18.215	0.908303727	Beta-mannosidase isoform X1
ncbi_103513412	5.190	8.210	0.661613601	Beta-mannosidase-like
ncbi_103516702	0.349	0.001	−8.445704636	Cathepsin L-like
ncbi_103517987	2.509	6.644	1.404939603	Cystatin-C-like isoform X2
ncbi_113466007	7.040	3.028	−1.217051415	Uncharacterised protein LOC113466007
ncbi_113469131	1.538	2.889	0.909035589	Beta-mannosidase-like
ncbi_113471436	8.308	3.420	−1.280306399	Sphingomyelin phosphodiesterase-like isoform X1
Xenobiotics biodegradation and metabolism				
ncbi_103508267	0.001	0.819	9.6783067	UDP-glucuronosyltransferase 2B20-like
ncbi_103509301	2.895	1.495	−0.953573448	Uncharacterised protein LOC103509301
MSTRG.25624	1.409	0.164	−3.103245156	Indole-3-acetaldehyde oxidase-like
ncbi_103519471	0.637	6.890	3.434453755	Cytochrome P450 4C1
ncbi_103505605	5.033	8.037	0.675393871	Uncharacterised protein LOC103505605
ncbi_103516373	2.317	4.529	0.966833136	Probable cytochrome P450 4d21
ncbi_103517030	114.875	66.375	−0.791353	Esterase FE4-like isoform X1
ncbi_103508266	1.046	1.829	0.80590927	UDP-glucuronosyltransferase 2B20-like
ncbi_103519760	7.255	4.069	−0.834485808	cGMP-specific 3′,5′-cyclic phosphodiesterase-like
ncbi_103510447	5.262	2.833	−0.893372035	Acyl-coenzyme A thioesterase 9, mitochondrial-like
ncbi_103508056	3.379	1.621	−1.059415622	1-Phosphatidylinositol 4,5-bisphosphate phosphodiesterase classes I and II-like
ncbi_113471436	8.308	3.420	−1.280306399	Sphingomyelin phosphodiesterase-like isoform X1

Table 5. Candidate genes identified from the SG transcriptomes of ACP

Gene names	Number of unigenes in *D. citri* SG
Vitellogenin	17
Heat shock protein 83-like	8
Trehalase	7
Esterase FE4-like	7
Serine/threonine-protein kinase	6
EF-hand domain-containing protein	5
Troponin T	5
Trehalose transporter Tret1-like	4
Mucin-12	3
Glycogen Synthase Kinase 3	2
Kinesin-like protein KIF3B	2
UDP-glucuronosyltransferase 2B20-like	2
Beta-galactosidase-like	2
Cuticle protein LPCP-23-like	1
Dual oxidase	1

abundant transcript encodes a mucin-5AC-like protein with an average FPKM value of 8597.05 (table S6). In addition, one digestive system-related pathway, salivary secretion, was found to be significantly enriched in the top 20 pathways in KEGG (fig. 7, table S6). Among these pathways, ten DEGs were significantly downregulated after *CL*as infection. These results indicated that the *CL*as pathogen may manipulate the secretory activity of saliva in the SG to alter the feeding behaviour of its psyllid vector. Interestingly, recent studies have revealed the potential roles of Mul in salivary sheath formation and modulation of plant defence responses (Shangguan *et al.*, 2018; Huo *et al.*, 2022; Liu *et al.*, 2022). Thus, these mucin-like proteins may also play dual roles in the formation of salivary sheath and response to plant immune defence in the SG of *D. citri*.

In summary, by using comparative transcriptomic analysis, we identified 861 DEGs between the SG of *CL*as-free and *CL*as-infected ACP colonies. The results of functional analysis revealed that *CL*as made noticeable effects on the SG during infection involved in host recognition, the immune response, nutrient and detoxification metabolism, and salivary secretion. This study provides scientific insights into the further research on the response mechanisms of the citrus psyllid to the invasion of *CL*as, which is much valuable for the formulation of consistent control strategy of citrus psyllid.

References

Ahmed S, Seo K and Kim Y (2021) An ovary-specific mucin is associated with choriogenesis mediated by prostaglandin signaling in *Spodoptera exigua*. *Archives of Insect Biochemistry and Physiology* **106**, e21748.

Aljbory Z and Chen MS (2018) Indirect plant defense against insect herbivores: a review. *Insect Science* **25**, 2–23.

Ammar ED, Shatters RG and Hall DG (2011*a*) Localization of *Candidatus* Liberibacter asiaticus, associated with citrus Huanglongbing disease, in its psyllid vector using fluorescence *in situ* hybridization. *Journal of Phytopathology* **159**, 726–734.

Ammar ED, Shatters RG, Lynch C and Hall DG (2011*b*) Detection and relative titer of *Candidatus* Liberibacter asiaticus in the salivary glands and alimentary canal of *Diaphorina citri* (Hemiptera: Psyllidae) vector of citrus Huanglongbing disease. *Annals of the Entomological Society of America* **104**, 526–533.

Andrade MO, Pang ZQ, Achor DS, Wang H, Yao TS, Singer BH and Wang N (2020) The flagella of '*Candidatus* Liberibacter asiaticus' and its movement in planta. *Molecular Plant Pathology* **21**, 109–123.

Benoit B, Baillet A and Poüs C (2021) Cytoskeleton and associated proteins: pleiotropic JNK substrates and regulators. *International Journal of Molecular Sciences* **22**, 8375.

Bromberger T, Zhu L, Klapproth S, Qin J and Moser M (2019) Rap1 and membrane lipids cooperatively recruit talin to trigger integrin activation. *Journal of Cell Science* **132**, jcs235531.

Brumin M, Lebedev G, Kontsedalov S and Ghanim M (2020) Levels of the endosymbiont Rickettsia in the whitefly *Bemisia tabaci* are influenced by the expression of vitellogenin. *Insect Molecular Biology* **29**, 241–255.

Canale MC, Tomaseto AF, Haddad MD, Della Coletta H and Lopes JRS (2017) Latency and persistence of '*Candidatus* Liberibacter asiaticus' in its psyllid vector, *Diaphorina citri* (Hemiptera: Liviidae). *Phytopathology* **107**, 264–272.

Carolan JC, Caragea D, Reardon KT, Mutti NS, Dittmer N, Pappan K, Cui F, Castaneto M, Poulain J, Dossat C, Tagu D, Reese JC, Reeck GR, Wilkinson TL and Edwards OR (2011) Predicted effector molecules in the salivary secretome of the pea aphid (*Acyrthosiphon pisum*): a dual transcriptomic/proteomic approach. *Journal of Proteome Research* **10**, 1505–1518.

Chen Q, Li ZQ, Liu SL, Chi YH, Jia DS and Wei TY (2022) Infection and distribution of *Candidatus* Liberibacter asiaticus in citrus plants and psyllid vectors at the cellular level. *Microbial Biotechnology* **15**, 1221–1234.

Chen JJ, Guo PH, Li YY, He WW, Chen WB, Shen ZJ, Zhang MS, Mao JJ and Zhang LS (2023) Cathepsin L contributes to reproductive diapause by regulating lipid storage and survival of *Coccinella septempunctata* (Linnaeus). *International Journal of Molecular Sciences* **24**, 611.

Coletta HD, Daugherty MP, Ferreira C and Lopes JRS (2014) Temporal progression of '*Candidatus* Liberibacter asiaticus' infection in citrus and acquisition efficiency by *Diaphorina citri*. *Phytopathology* **104**, 416–421.

Colonne PM, Winchell CG and Voth DE (2016) Hijacking host cell highways: manipulation of the host actin cytoskeleton by obligate intracellular bacterial pathogens. *Frontiers in Cellular and Infection Microbiology* **6**, 107.

da Graca JV, Douhan GW, Halbert SE, Keremane ML, Lee RF, Vidalakis G and Zhao HW (2016) Huanglongbing: an overview of a complex pathosystem ravaging the world's citrus. *Journal of Integrative Plant Biology* **58**, 373–387.

DeLay B, Mamidala P, Wijeratne A, Wijeratne S, Mittapalli O, Wang J and Lamp W (2012) Transcriptome analysis of the salivary glands of potato leafhopper, *Empoasca fabae*. *Journal of Insect Physiology* **58**, 1626–1634.

Duan YP, Zhou LJ, Hall DG, Li WB, Doddapaneni H, Lin H, Liu L, Vahling CM, Gabriel DW, Williams KP, Dickerman A, Sun YJ and Gottwald T (2009) Complete genome sequence of citrus Huanglongbing bacterium, 'Liberibacter asiaticus' obtained through metagenomics. *Molecular Plant–Microbe Interactions* **22**, 1011–1020.

Galdeano DM, Pacheco ID, Alves GR, Granato LM, Rashidi M, Turner D, Levy A and Machado MA (2020) Friend or foe? Relationship between 'Candidatus Liberibacter asiaticus' and *Diaphorina citri*. *Tropical Plant Pathology* **45**, 559–571.

Gao LJ, Qiao HH, Wei P, Moussian B and Wang YW (2022) Xenobiotic responses in insects. *Archives of Insect Biochemistry and Physiology* **109**, e21869.

George J, Ammar ED, Hall DG and Lapointe SL (2017) Sclerenchymatous ring as a barrier to phloem feeding by Asian citrus psyllid: evidence from electrical penetration graph and visualization of stylet pathways. *PLoS ONE* **12**, e0173520.

George J, Ammar E, Hall DG, Shatters RG and Lapointe SL (2018) Prolonged phloem ingestion by *Diaphorina citri* nymphs compared to adults is correlated with increased acquisition of citrus greening pathogen. *Scientific Reports* **8**, 10352.

Ghanim M, Fattah-Hosseini S, Levy A and Cilia M (2016) Morphological abnormalities and cell death in the Asian citrus psyllid (*Diaphorina citri*) midgut associated with *Candidatus* Liberibacter asiaticus. *Scientific Reports* **6**, 33418.

Ghosh S, Jassar O, Kontsedalov S, Lebedev G, Wang CX, Turner D, Levy A and Ghanim M (2019) A transcriptomics approach reveals putative interaction of Liberibacter solanacearum with the endoplasmic reticulum of its psyllid vector. *Insects* **10**, 279.

Giron D, Huguet E, Stone GN and Body M (2016) Insect-induced effects on plants and possible effectors used by galling and leaf-mining insects to manipulate their host-plant. *Journal of Insect Physiology* **84**, 70–89.

Gouin E, Welch MD and Cossart P (2005) Actin-based motility of intracellular pathogens. *Current Opinion in Microbiology* **8**, 35–45.

Grumati P and Dikic I (2018) Ubiquitin signaling and autophagy. *Journal of Biological Chemistry* **293**, 5404–5413.

Guo HJ, Zhang YJ, Tong JH, Ge PP, Wang QY, Zhao ZH, Zhu-Salzman K, Hogenhout SA, Ge F and Sun YC (2020) An aphid-secreted salivary protease activates plant defense in phloem. *Current Biology* **30**, 4826–4836.e4827.

Hall DG, Richardson ML, Ammar ED and Halbert SE (2013) Asian citrus psyllid, *Diaphorina citri*, vector of citrus Huanglongbing disease. *Entomologia Experimentalis et Applicata* **146**, 207–223.

Han SP, Wang D, Song P, Zhang S and He YZ (2022) Molecular characterization of vitellogenin and its receptor in *Spodoptera frugiperda* (J. E. Smith, 1797), and their function in reproduction of female. *International Journal of Molecular Sciences* **23**, 11972.

Huo Y, Zhao J, Meng XY, Yang J, Zhang ZY, Liu ZW, Fang RX and Zhang LL (2022) *Laodelphax striatellus* saliva mucin enables the formation of stylet sheaths to facilitate its feeding and rice stripe virus transmission. *Pest Management Science* **78**, 3498–3507.

Iordachescu M and Imai R (2008) Trehalose biosynthesis in response to abiotic stresses. *Journal of Integrative Plant Biology* **50**, 1223–1229.

Ji R, Yu HX, Fu Q, Chen HD, Ye WF, Li SH and Lou YG (2013) Comparative transcriptome analysis of salivary glands of two populations of rice brown planthopper, *Nilaparvata lugens*, that differ in virulence. *PLoS ONE* **8**, e79612.

Ji R, Fu JM, Shi Y, Li J, Jing MF, Wang L, Yang SY, Tian T, Wang LH, Ju JF, Guo HF, Liu B, Dou DL, Hoffmann AA, Zhu-Salzman K and Fang JC (2021) Vitellogenin from planthopper oral secretion acts as a novel effector to impair plant defenses. *New Phytologist* **232**, 802–817.

Kaur N, Chen W, Zheng Y, Hasegawa DK, Ling KS, Fei Z and Wintermantel WM (2017) Transcriptome analysis of the whitefly, *Bemisia tabaci* MEAM1 during feeding on tomato infected with the crinivirus, *Tomato chlorosis* virus, identifies a temporal shift in gene expression and differential regulation of novel orphan genes. *BMC Genomics* **18**, 370.

Killiny N, Hijaz F, Ebert TA and Rogers ME (2017) A plant bacterial pathogen manipulates its insect vector's energy metabolism. *Applied and Environmental Microbiology* **83**, e03005.

Kruse A, Fattah-Hosseini S, Saha S, Johnson R, Warwick E, Sturgeon K, Mueller L, MacCoss MJ, Shatters RG and Heck MC (2017) Combining 'omics and microscopy to visualize interactions between the Asian citrus psyllid vector and the Huanglongbing pathogen *Candidatus* Liberibacter asiaticus in the insect gut. *PLoS ONE* **12**, e0179531.

Kruse A, Ramsey JS, Johnson R, Hall DG, MacCoss MJ and Heck M (2018) *Candidatus* Liberibacter asiaticus minimally alters expression of immunity and metabolism proteins in hemolymph of *Diaphorina citri*, the insect vector of Huanglongbing. *Journal of Proteome Research* **17**, 2995–3011.

Lai KK, Davis-Richardson AG, Dias R and Triplett EW (2016) Identification of the genes required for the culture of, the closest cultured relative of the plant pathogens. *Frontiers in Microbiology* **7**, 547.

Ligeon LA, Temime-Smaali N and Lafont F (2011) Ubiquitylation and autophagy in the control of bacterial infections and related inflammatory responses. *Cellular Microbiology* **13**, 1303–1311.

Liu K, He JW, Guan ZY, Zhong MZ, Pang R and Han QX (2021) Transcriptomic and metabolomic analyses of *Diaphorina citri* Kuwayama infected and non-infected With *Candidatus* Liberibacter asiaticus. *Frontiers in Physiology* **11**, 630037.

Liu YD, Yi JY, Jia HK, Miao YT and Hou ML (2022) *Sogatella furcifera* saliva mucin-like protein Is required for feeding and induces rice defences. *International Journal of Molecular Sciences* **23**, 8239.

Lou YH, Shen Y, Li DT, Huang HJ, Lu JB and Zhang CX (2019) A mucin-like protein is essential for oviposition in *Nilaparvata lugens*. *Frontiers in Physiology* **10**, 551.

Lu K, Song YY and Zeng RS (2021) The role of cytochrome P450-mediated detoxification in insect adaptation to xenobiotics. *Current Opinion in Insect Science* **43**, 103–107.

Mann M, Fattah-Hosseini S, Ammar E, Stange R, Warrick E, Sturgeon K, Shatters R and Heck M (2018) *Diaphorina citri* nymphs are resistant to morphological changes induced by 'Candidatus Liberibacter asiaticus' in midgut epithelial cells. *Infection and Immunity* **86**, e00889–e00817.

Matsumoto Y and Hattori M (2018) The green rice leafhopper, *Nephotettix cincticeps* (Hemiptera: Cicadellidae), salivary protein NcSP75 is a key effector for successful phloem ingestion. *PLoS ONE* **13**, e0202492.

Matsumoto Y, Suetsugu Y, Nakamura M and Hattori M (2014) Transcriptome analysis of the salivary glands of *Nephotettix cincticeps* (Uhler). *Journal of Insect Physiology* **71**, 170–176.

Maywald ML, Picciotto C, Lepa C, Bertgen L, Yousaf FS, Ricker A, Klingauf J, Krahn MP, Pavenstadt H and George B (2022) Rap1 activity is essential for focal adhesion and slit diaphragm integrity. *Frontiers in Cell and Developmental Biology* **10**, 790365.

Mukherjee R and Dikic I (2022) Regulation of host–pathogen interactions via the ubiquitin system. *Annual Review of Microbiology* **76**, 211–233.

Munir S, He PF, Wu YX, He PB, Khan S, Huang M, Cui WY, He PJ and He YQ (2018) Huanglongbing control: perhaps the end of the beginning. *Microbial Ecology* **76**, 192–204.

Munro P, Flatau G and Lemichez E (2007) Bacteria and the ubiquitin pathway. *Current Opinion in Microbiology* **10**, 39–46.

Peng T, Yuan YZ, Huang AJ, He J, Fu SM, Duan S, Yi L, Yuan CY, Yuan HZ, Wang XF and Zhou CY (2023) Interaction between the flagellum of *Candidatus* Liberibacter asiaticus and the vitellogenin-like protein of *Diaphorina citri* significantly influences CLas titer. *Frontiers in Microbiology* **14**, 1119619.

Perilla-Henao LM and Casteel CL (2016) Vector-borne bacterial plant pathogens: interactions with hemipteran insects and plants. *Frontiers in Plant Science* **7**, 1163.

Ramsey JS, Chavez JD, Johnson R, Hosseinzadeh S, Mahoney JE, Mohr JP, Robison F, Zhong X, Hall DG, MacCoss M, Bruce J and Cilia M (2017) Protein interaction networks at the host–microbe interface in *Diaphorina citri*, the insect vector of the citrus greening pathogen. *Royal Society Open Science* **4**, 160545.

Rao WW, Zheng XH, Liu BF, Guo Q, Guo JP, Wu Y, Shangguan XX, Wang HY, Wu D, Wang ZZ, Hu L, Xu CX, Jiang WH, Huang J, Shi SJ and He GC (2019) Secretome analysis and in planta expression of salivary proteins identify candidate effectors from the brown planthopper *Nilaparvata lugens*. *Molecular Plant–Microbe Interactions* **32**, 227–239.

Sarkar P and Ghanim M (2022) Interaction of *Liberibacter solanacearum* with host psyllid vitellogenin and its association with autophagy. *Microbiology Spectrum* **10**, e0157722.

Sarkar P, Kontsedalov S, Lebedev G and Ghanim M (2021) The actin cytoskeleton mediates transmission of 'Liberibacter solanacearum' by the carrot psyllid. *Applied and Environmental Microbiology* **87**, e02393-20.

Shangguan XX, Zhang J, Liu BF, Zhao Y, Wang HY, Wang ZZ, Guo JP, Rao WW, Jing SL, Guan W, Ma YH, Wu Y, Hu L, Chen RZ, Du B, Zhu LL, Yu DZ and He GC (2018) A mucin-like protein of planthopper is required for feeding and induces immunity response in plants. *Plant Physiology* **176**, 552–565.

Shokrollah H, Abdullah TL, Sijam K and Abdullah SNA (2010) Ultrastructures of *Candidatus* Liberibacter asiaticus and its damage in Huanglongbing (HLB) infected citrus. *African Journal of Biotechnology* **9**, 5897–5901.

Shukla E, Thorat LJ, Nath BB and Gaikwad SM (2015) Insect trehalase: physiological significance and potential applications. *Glycobiology* **25**, 357–367.

Slisz AM, Breksa AP, Mishchuk DO, McCollum G and Slupsky CM (2012) Metabolomic analysis of citrus infection by 'Candidatus Liberibacter' reveals insight into pathogenicity. *Journal of Proteome Research* **11**, 4223–4230.

Spallek T, Robatzek S and Gohre V (2009) How microbes utilize host ubiquitination. *Cellular Microbiology* **11**, 1425–1434.

Su YL, Li JM, Li M, Luan JB, Ye XD, Wang XW and Liu SS (2012) Transcriptomic analysis of the salivary glands of an invasive whitefly. *PLoS ONE* **7**, e39303.

Sun YX, Zhu BJ, Tang L, Sun Y, Chen C, Abbas MN, Wang L, Qian C, Wei GQ and Liu CL (2017) Cathepsin o is involved in the innate immune response and metamorphosis of *Antheraea pernyi*. *Journal of Invertebrate Pathology* **150**, 6–14.

Sun YX, Tang L, Wang P, Abbas MN, Tian JW, Zhu BJ and Liu CL (2018) Cathepsin L-like protease can regulate the process of metamorphosis and fat body dissociation in *Antheraea pernyi*. *Developmental and Comparative Immunology* **78**, 114–123.

Swatek KN and Komander D (2016) Ubiquitin modifications. *Cell Research* **26**, 399–422.

Tang XT and Tamborindeguy C (2020) No evidence of apoptotic response of the potato psyllid to 'Liberibacter solanacearum' at the gut interface. *Infection and Immunity* **88**, e00242-19.

Tiwari S, Pelz-Stelinski K, Mann RS and Stelinski LL (2011) Glutathione transferase and cytochrome P (general oxidase) activity levels in Liberibacter asiaticus-infected and uninfected Asian citrus psyllid (Hemiptera: Psyllidae). *Annals of the Entomological Society of America* **104**, 297–305.

Vanaclocha P, Jones MM, Tansey JA, Monzo C, Chen XL and Stansly PA (2019) Residual toxicity of insecticides used against the Asian citrus psyllid and resistance management strategies with thiamethoxam and abamectin. *Journal of Pest Science* **92**, 871–883.

van Bell AJE and Will T (2016) Functional evaluation of proteins in watery and gel saliva of aphids. *Frontiers in Plant Science* **7**, 1840.

Vyas M, Fisher TW, He RF, Nelson W, Yin GH, Cicero JM, Willer M, Kim R, Kramer R, May GA, Crow JA, Soderlund CA, Gang DR and Brown JK (2015) Asian citrus psyllid expression profiles suggest Liberibacter asiaticus-mediated alteration of adult nutrition and metabolism, and of nymphal development and immunity. *PLoS ONE* **10**, e0130328.

Wang G, Gou YP, Guo SF, Zhou JJ and Liu CZ (2021) RNA interference of trehalose-6-phosphate synthase and trehalase genes regulates chitin metabolism in two color morphs of *Acyrthosiphon pisum* Harris. *Scientific Reports* **11**, 948.

Wen ZY, Zhang Y, Lin ZK, Shi K and Jiu YM (2020) Cytoskeleton – a crucial key in host cell for coronavirus infection. *Journal of Molecular Cell Biology* **12**, 968–979.

Wu TY, Luo XZ, Xu CB, Wu FN, Qureshi JA and Cen YJ (2016) Feeding behavior of and its transmission of 'Liberibacter asiaticus' to citrus. *Entomologia Experimentalis et Applicata* **161**, 104–111.

Xu HX, Qian LX, Wang XW, Shao RX, Hong Y, Liu SS and Wang XW (2019) A salivary effector enables whitefly to feed on host plants by eliciting salicylic acid-signaling pathway. *Proceedings of the National Academy of Sciences of the United States of America* **116**, 490–495.

Xu JJ, Chang YM, Lu M, Tie Y, Dong YL, Chen GY, Ma ZQ, Liu XL and Li YQ (2021) Two single mutations in carboxylesterase 001C improve fenvalerate hydrolase activity in *Helicoverpa armigera*. *Pesticide Biochemistry and Physiology* **179**, 104969.

Yang CH, Guo JY, Chu D, Ding TB, Wei KK, Cheng DF and Wan FH (2017) Secretory laccase 1 in *Bemisia tabaci* MED is involved in whitefly–plant interaction. *Scientific Reports* **7**, 3623.

Yang H, Zhang RZ, Zhang YH, Liu Q, Li Y, Gong J and Hou Y (2020) Cathepsin-L is involved in degradation of fat body and programmed cell death in *Bombyx mori*. *Gene* **760**, 144998.

Yasugi T, Yamada T and Nishimura T (2017) Adaptation to dietary conditions by trehalose metabolism in *Drosophila*. *Scientific Reports* **7**, 1619.

Yu XD and Killiny N (2018) The secreted salivary proteome of Asian citrus psyllid *Diaphorina citri*. *Physiological Entomology* **43**, 324–333.

Yu HZ, Huang YL, Li NY, Xie YX, Zhou CH and Lu ZJ (2019) Potential roles of two cathepsin genes, DcCath-L and DcCath-O in the innate immune response of *Diaphorina citri*. *Journal of Asia-Pacific Entomology* **22**, 1060–1069.

Yu HZ, Li NY, Zeng XD, Song JC, Yu XD, Su HN, Chen CX, Yi L and Lu ZJ (2020) Transcriptome analyses of *Diaphorina citri* midgut responses to *Candidatus* Liberibacter asiaticus infection. *Insects* **11**, 171.

Zhang Y, Fan J, Sun JR, Francis F and Chen JL (2017) Transcriptome analysis of the salivary glands of the grain aphid, *Sitobion avenae*. *Scientific Reports* **7**, 15911.

Zhao L, Yang M, Shen Q, Liu X, Shi Z, Wang S and Tang B (2016) Functional characterization of three trehalase genes regulating the chitin metabolism pathway in rice brown planthopper using RNA interference. *Scientific Reports* **6**, 27841.

Zhao XM, Zhang J, Yang JP, Niu N, Zhang JZ and Yang Q (2020) Mucin family genes are essential for the growth and development of the migratory locust, *Locusta migratoria*. *Insect Biochemistry and Molecular Biology* **123**, 103404.